AN ABSTRACT OF THE THESIS OF

Long Ren Chen for the degree of Master of Science in Electrical and Computer Engineering presented on June 14 , 1990.
Title: An Adaptive Pitch Axis Autopilot Design For An Unstable Nonminimum Phase Pitch Axis Model

Abstract approved: Redacted for Privacy
John L. Baugen

An adaptive pitch axis autopilot design procedure is presented. The design procedure is applicable to both stable and unstable pitch axis models and to those having nonminimum phase. The design approach assumes the adaptive autopilot is activated after achieving level flight. It is shown a rate-feedback compensator can be designed to ensure stable level flight pitch axis operation for the entire desired flight regime. The adaptive control loop design utilizes a pole-placement algorithm. The closed-loop characteristic polynomial is designed to have dominant poles of that of an ideal second order system to obtain the desired transient response. The identification of the system uses a modified least-squares algorithm with a variable forgetting factor. The nonlinear pitch axis model is used in simulations to evaluate the design. Command response tests include the step response and the ramp command response.

Simulation results indicate that the adaptive pitch axis autopilot is capable of tracking altitude commands after activation. The closed-loop system response is close to that of the ideal second order system having the dominant poles.

AN ADAPTIVE PITCH AXIS AUTOPILOT DESIGN FOR AN UNSTABLE NONMINIMUM PHASE PITCH AXIS MODEL

By

Long Ren Chen

A THESIS

Submitted to

Oregon State University

in partial fulfillment of

the requirements for the

degree of

Master of Science

Completed June 14, 1990

Commencement June 1991

APPROVED:

Redacted for Privacy

Professor of Electrical & Computer Engineering in Charge of Major

Redacted for Privacy

Head of Department of Electrical & Computer Engineering

Redacted for Privacy

Dean of Graduate School

Date thesis is presented June 14, 1990

Type by Long Ren Chen for Long Ren Chen

ACKNOWLEDGEMENT

This thesis could not have been completed without the help of several people. First, my parents, Dong-Zhi Chen and Jin-Qing Lei, gave me support and encouragement throughout my education. My wife Dan-Tong Zhu, has been my friend, helpmate and encourager. My major professor John Saugen, guided my studies and gave his critical review and comments in the preparation of this manuscript. Professor Ron Mohler, Professor Roy Rathja and Professor John Nabeleck, served as my graduate committee members and gave me valuable advice. Special thanks are due to our friends Miss Felice McKinnon and Grandma Veda McKinnon, who provided us housing with comfortable surroundings.

Finally, I would like to express my appreciation to my other family members — especially my sister Feng-Ping Chen and my brother Long-Yi Chen for their help and encouragement.

TABLE OF CONTENTS

TABLE OF CONTENTS (Continued)

LIST OF FIGURES

LIST OF TABLES

AN ADAPTIVE PITCH AXIS AUTOPILOT DESIGN FOR AN UNSTABLE NONMININUM PHASE PITCH AXIS MODEL

CHAPTER 1

INTRODUCTION

In classical control designs, the process models are assumed fixed and thus the parameters of the controller are taken as constants. However, variations in the process models occur frequently; hence the applications of classical controllers are thus restricted. In adaptive control the process model is identified on-line and the controller parameters are automatically adjusted in response to the change of the process model. As one of the important applications of adaptive control, the adaptive autopilot has been intensively studied for more than a decade. This chapter gives a brief description of the conventional pitch axis autopilot designs and limitations, approaches in the adaptive autopilot designs, the objective and outline of the thesis.

1.1 Conventional Pitch Axis Autopilot Designs and Limitations

A typical way of designing an aircraft autopilot is to design a compensator for the aircraft based on a linearized aircraft model. The linearized aircraft model is determined by linearizing the aircraft model around an operating point under the assumption that the operating point

of the flight is fixed. Techniques such as the Nyquist compensation method and root-locus technique can be applied in the design of such a compensator. For example, the root-locus technique is applied in the autopilot designs in Blakelock [1965] and in Saugen [1987]. The autopilot designs generally assumed that the parameters of the linearized aircraft transfer function do not change with the variation of the speed, the altitude, and the weight of the aircraft. In fact, the poles and zeros of the aircraft transfer functions depend greatly on the speed and altitude of the aircraft. In reality and especially for high performance aircraft, the speed and altitude change frequently. So, the parameters of the aircraft model change if the aircraft is not limited to a horizontal flight path with a constant speed.

The transient response of an aircraft depends upon the parameters of the compensated aircraft flight control system. Consequently one solution to the varying parameter problem is to schedule the parameters as a function of Mach number or dynamic pressure. This approach requires extensive system analysis a priori to determine the autopilot parameters for the various flight conditions. To perform this analysis the aerodynamic data for the entire flight regime much be known accurately. This information is usually obtained from wind tunnel tests of scale models of the aircraft. After the aircraft is built, provision is made for changing the autopilot gains in flight. This procedure is then followed by extensive flight testing to determine the final optimum gain settings. The analysis and design procedure is time consuming and expensive. Furthermore, this approach lacks robustness in flight due to system modeling errors.

1.2 Approaches in Adaptive Autopilot Designs

An adaptive control system is a special compensator which is capable of tuning itself to optimal settings and is also capable of retuning itself should the system dynamics subsequently change. So, an adaptive controller can be applied to solve the parameter variation problem of the aircraft system.

A typical adaptive autopilot is shown in Figure 1-1. It can be regarded as being composed of an inner loop and an outer loop. The inner loop is the basic control loop which consists of the controller and the aircraft dynamics. The outer loop is composed of a parameter estimator and an adaptive process algorithm. The parameter estimator estimates the parameters of the aircraft system using the sampled data of the input and output of the aircraft system. The adaptive process algorithm adjusts the parameters of the controller in the inner loop to yield desired system output.

The idea of the adaptive autopilot has been around for about two decades. Many basic configurations for adaptive autopilots were proposed in 1950s as introduced in Blakelock [1966]. However, early attempts at adaptive autopilot design were largely unsuccessful because the supporting theory was essentially nonexistent and there were also difficulties in implementation since computer technology was still in its infancy.

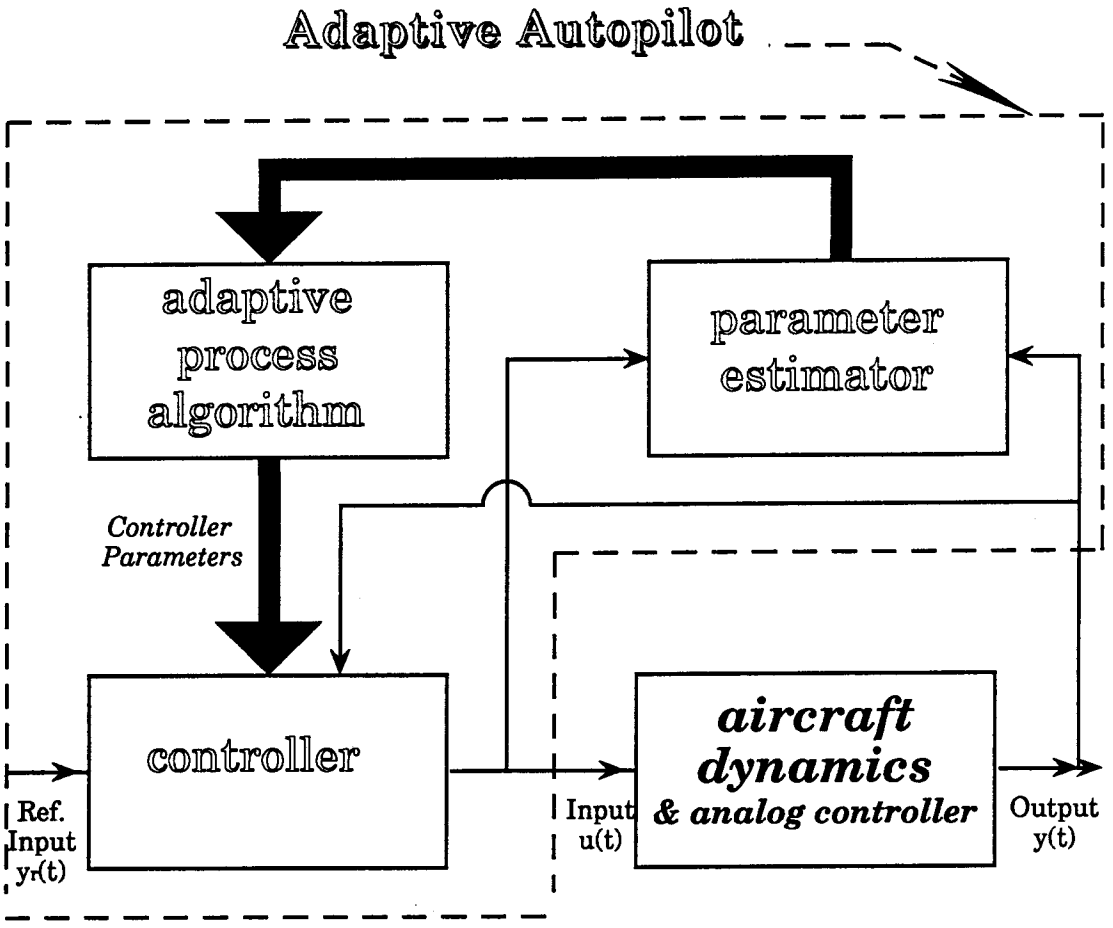

Figure 1.1 Block Diagram of the Adaptive Controller.

During the 1960s there were major developments in system identification and control theory. This led to an improved understanding of the general problem of the adaptive autopilot and spurred renewed interest in the topic. Different adaptive design methods are reported in the special issue of *the IEEE Transactions on Automatic Control* (1977, Vol. AC-22, No.5). The adaptive autopilot designs are mostly based on the linearized aircraft model. Examples of simulations occur in the literatures which show that the adaptive autopilot is effective in achieving desired system performance. However, there are problems when the aircraft dynamics has nonminimum phase* . Simulations for such systems show that adaptive autopilots based on common adaptive algorithms are unable to control the nonminimum phase system. See John *et al* [1982].

1.3 Objective and Outline of the Thesis

An adaptive controller design procedure is applied to the aircraft pitch axis model presented in Appendix I. The linearized model has nonminimum phase as shown in Chapter 2. The adaptive pitch axis autopilot design method used here employs a pole-placement algorithm utilizing a parameter estimator based on a modified least square identification algorithm. Further details on the design method are presented in Chapter 4. The objective of the thesis is to test the

---

* A physical system has nonminimum phase if its Laplace transfer function has one or more right-half plane zeros or poles. For a discrete-time Z-transfer function the zeros or poles are outside the unit circle in the complex Z-domain.

effectiveness of the adaptive controller in maintaining desired transient response as well as maintaining tracking performance.

As a design approach, the adaptive autopilot is designed to be activated after the aircraft has achieved level flight after taking off. The adaptive controller then operates continuously for subsequent flight maneuver. As shown in Chapter 2, the linearized pitch axis model of the assumed aircraft is an unstable nonminimum phase system. So, prior to the design of the adaptive autopilot, the system is stabilized for all level flight conditions. Rate-feedback compensation is found to be effective in stabilizing the unstable aircraft system for the desired flight envelope. However, rate-feedback does not achieve desired system behavior for all desired flight conditions. This is discussed in Chapter 3.

If a feedback system has a feedforward transfer function which has nonminimum phase zeros, then the feedback system will also have nonminimum phase zeros. Therefore, the nonminimum phase nature of the linearized pitch axis aircraft system is carried over to the feedback system. Furthermore, a nonminimum phase continuous system generally produces a nonminimum phase discrete system (Clarke [1984]). Clarke discusses how a long sample interval can sometimes be used to avoid the nonminimum phase zero(s). However, the corresponding control is extremely poor. Consequently, it is important that a digital autopilot be designed using the nonminimum phase discrete system model.

Since the discrete pitch axis system model of the aircraft is a nonminimum phase system, caution is required in the selection of an adaptive algorithm. Early self-turning regulators and model reference adaptive control (MRAC) algorithms involve pole-zero cancellations with the result that the cancelled system zeros are factors of the closed-loop characteristic equation (Clarke[1984]). A nonminimum phase system has at least one nonminimum phase zero which can be "cancelled" by an unstable pole. So, the adaptive algorithm based on a conventional self-tuning regulator or a MRAC algorithm is not considered for the nonminimum phase aircraft system. A pole-placement algorithm proposed by Astrom & Wittenmark [1980][1984] is applied in this study. It is shown in Astrom & Wittenmark that the algorithm is adequate for a nonminimum phase discrete system and generally results in good tracking. Modifications are also included to track the input with minimum error. A modified least-square identification algorithm is used in the design, rather than the ordinary least-square algorithm that is used in Astrom & Wittenmark. This is discussed in Chapter 4.

Simulations of the designed adaptive autopilot are included which show the transient response of the aircraft system and the effect of the modified least-square algorithm on altitude tracking. The simulations use the nonlinear aircraft model of Chapter 2. Details are discussed in Chapter 5.

CHAPTER 2

THE PITCH AXIS SYSTEM AND THE DESIRED BEHAVIOR

In this chapter, the aircraft model studied is introduced. The pitch axis system transfer function is found through linearization. The desired behavior of the system is discussed. Design goal are defined.

2.1 The Pitch Axis System of the Aircraft

The aircraft model used for the study is shown in Figure 2.1 (also shown in Appendix I). The inertial reference axis system consists of a fixed horizontal axis and a vertical axis. Pitch rotation is taken positive in a counter-clockwise sense around the vehicle center of mass and is referred to the horizontal plane.

The following assumptions are used. The aircraft has a gross weight of 10,000 pounds, including the maximum weight of fuel. The average fuel consumed is 50 pounds per hour. The aircraft has an elevator for the purpose of pitch axis control. The actuator of the elevator is assumed ideal, that is, elevator dynamics are neglectable. The distance from the center of mass to the center of aerodynamic pressure, r_{cp}, is 0.5 feet and the distance from the center of mass to elevator center of aerodynamic pressure, r_e, is 20 feet. r_{cp} and r_e are as indicated in Figure 2.1. The thrust of the engine is assumed to be adjustable.

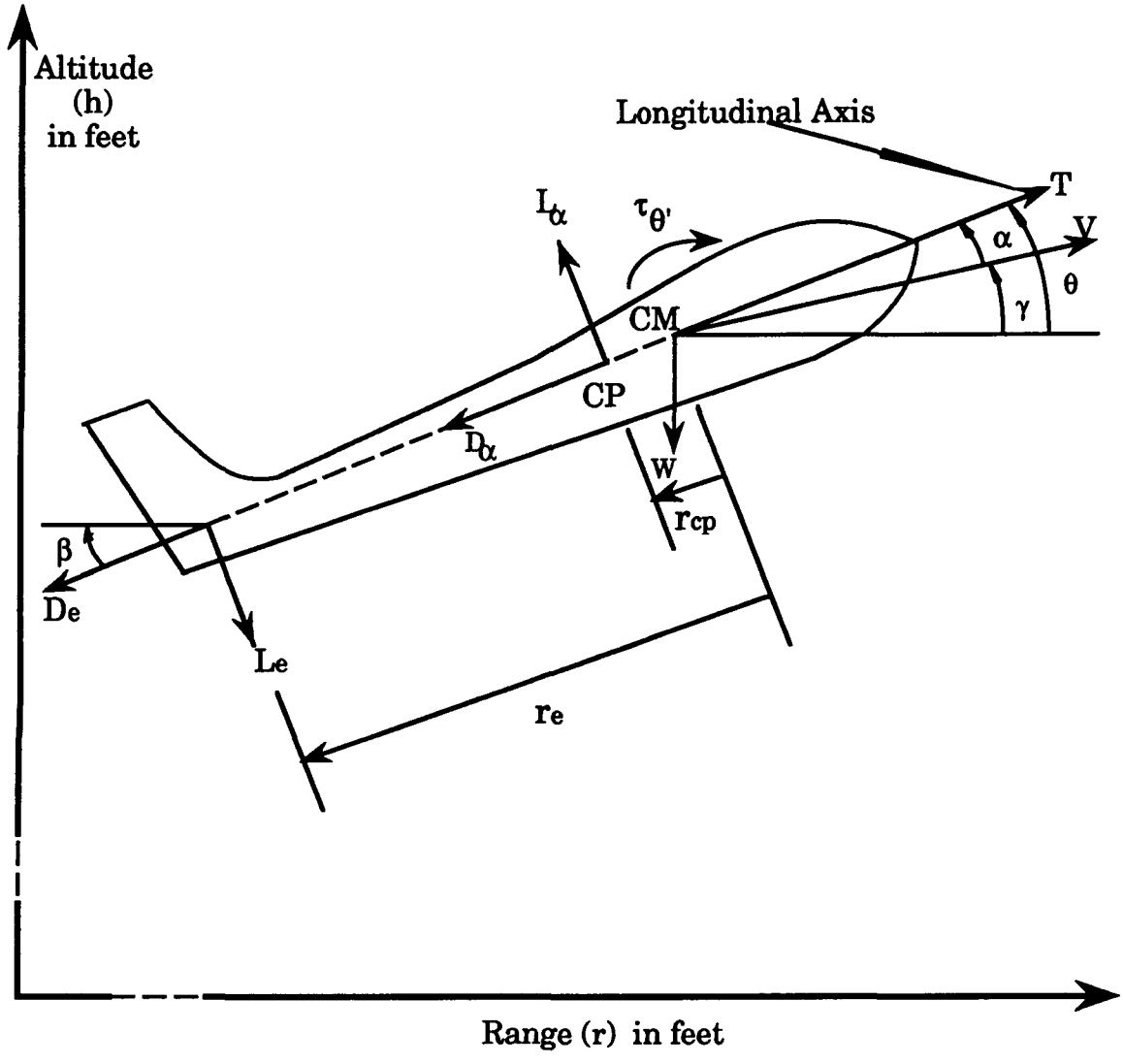

Figure 2.1 The Pitch Axis Aircraft Model.

The aircraft is assumed to fly between 0.5 Mach to 0.8 Mach. The maximum altitude of the aircraft is assumed to be 40,000 feet. The aerodynamic coefficients within the flight envelope are constants as shown in Table 2.1 (also in Appendix I).

Polar Moment of Inertia (J, in lb·ft·sec^2/rad)	6,000
Moment Coefficient ($c_{m\theta'}$, θ in deg./sec.)	1.544
Coefficient $c_{l\alpha}$, α in degree	13.96
Coefficient $c_{l\beta}$, β in degree	0.698
Coefficient $c_{d\alpha}$	10.00
Coefficient $c_{d\beta}$	0.500
Atmospheric Density at zero altitude (ρ_z, in Slugs/Cu.ft)	0.00238
Exponential Atmosphere Factor (H, in ft)	30,000

Table 2.1 Aircraft Pitch Axis Data and Environmental Parameters. (See Appendix I.)

2.1.1 The Pitch Axis System

The state variable model of the pitch axis system is given by Equation (2-1), which is the same as Equation (A.1) in Appendix I. Note that the system is non-linear.

The state variable model of the pitch axis system is:

$$\begin{cases} x' = \begin{bmatrix} r' \\ r'' \\ h' \\ h'' \\ \theta' \\ \theta'' \end{bmatrix} = \begin{bmatrix} \dot{x}_1 \\ \dot{x}_2 \\ \dot{x}_3 \\ \dot{x}_4 \\ \dot{x}_5 \\ \dot{x}_6 \end{bmatrix} = \begin{bmatrix} x_2 \\ k_r - c_\alpha \cdot (x_5 - \dfrac{x_4}{V}) \cdot x_5 + c_\beta u_1 x_5 \\ x_4 \\ k_r x_5 + c_\alpha \cdot (x_5 - \dfrac{x_4}{V}) - c_\beta u_1 - g \\ x_6 \\ -N_\theta \cdot x_6 - N_\alpha \cdot (x_5 - \dfrac{x_4}{V}) + N_\beta u_1 \end{bmatrix}; \\ q = \begin{bmatrix} h \\ \theta \end{bmatrix} = \begin{bmatrix} x_3 \\ x_5 \end{bmatrix}; \end{cases} \qquad (2\text{-}1)$$

where

$$\text{the state variable } x = \begin{bmatrix} x_1 \\ x_2 \\ x_3 \\ x_4 \\ x_5 \\ x_6 \end{bmatrix} = \begin{bmatrix} \text{range} \\ \text{horizontal speed} \\ \text{altitude} \\ \text{vertical speed} \\ \text{pitch angle} \\ \text{pitch rate} \end{bmatrix} = \begin{bmatrix} r \\ r' \\ h \\ h' \\ \theta \\ \theta' \end{bmatrix},$$

the input to the system $u = [u_1] = [\text{elevator angle}] = [\beta]$,

$$\text{the output of the system } q = \begin{bmatrix} q_1 \\ q_2 \end{bmatrix} = \begin{bmatrix} \text{altitude} \\ \text{pitch angle} \end{bmatrix} = \begin{bmatrix} h \\ \theta \end{bmatrix},$$

V is the speed of the aircraft, i.e., $V = \sqrt{r'^2 + h'^2} = \sqrt{x_2^2 + x_4^2}$, and g is the acceleration due to gravity ($g = 32.2$ ft/sec^2).

The parameters c_α, c_β, N_α, N_β, $N_{\theta'}$ & k_r in Equation (2-1) are defined in Appendix I:

$$c_\alpha = \frac{1}{m}(0.5\rho V^2)c_{l\alpha} \quad ; \qquad c_\beta = \frac{1}{m}(0.5\rho V^2)c_{l\beta} \quad ;$$

$$N_\alpha = \frac{m}{J} r_{cp} c_\alpha \quad ; \qquad N_\beta = \frac{m}{J} r_e c_\beta \quad ;$$

$$k_r = \frac{T}{m} - \frac{1}{m}(0.5\rho V^2)(c_{d\alpha} + c_{d\beta}) \quad ; \quad N_{\theta'} = (0.5\rho V^2)c_{m\theta'} \quad ;$$

where, ρ is the atmospheric density ($\rho = \rho_z e^{(-\frac{h}{H})}$) ;

r_e , r_{cp} are as shown Figure 2.1;

ρ_z, H, $c_{l\alpha}$, $c_{l\beta}$, $c_{d\alpha}$, $c_{d\beta}$, $c_{m\theta'}$ and J are given in Table 2.1.

2.1.2 The Linearized Pitch Axis Model

Assuming a constant velocity horizontal flight operating point, then $x^T = [r_0 \quad V \quad h_0 \quad 0 \quad \theta_0 \quad 0]$ with $u_0 = [\beta_0]$ and $q^T = [h_0 \quad \theta_0]$, where r_0, V, h_0, θ_0, and β_0 are constants which define the operating point. Horizontal flight requires h_0' and θ_0' to be zero. The following assumptions are also made for the operating point:

(1) The thrust and the weight of the aircraft are constants.

(2) The aerodynamics coefficients (as shown in Table 2.1) are constants.

(3) Dynamical motion around the operating point for small angles does not change significantly the magnitude of V. However, r' and h' will change although r' is still assumed to be close to V.

The linearized state variable model, as shown in Equation (A.3) of Appendix I is repeated in Equation (2-2):

$$\delta x' = \begin{bmatrix} 0 & 1 & 0 & 0 & 0 & 0 \\ 0 & 0 & a_{23} & a_{24} & a_{25} & 0 \\ 0 & 0 & 0 & 1 & 0 & 0 \\ 0 & 0 & a_{43} & a_{44} & a_{45} & 0 \\ 0 & 0 & 0 & 0 & 0 & 1 \\ 0 & 0 & a_{63} & a_{64} & a_{65} & a_{66} \end{bmatrix} \cdot \delta x + \begin{bmatrix} 0 \\ b_2 \\ 0 \\ b_4 \\ 0 \\ b_6 \end{bmatrix} \cdot \delta u \qquad (2\text{-}2)$$

$$\delta q = [1 \quad 1] \begin{bmatrix} x_3 \\ x_5 \end{bmatrix}$$

where, $\begin{cases} x = x_0 + \delta x \\ u = u_0 + \delta u \end{cases}$ and, the "a" and "b" parameters are given by Equation (A.5) in Appendix I.

As discussed in Appendix I, if the aircraft is flying horizontally at an altitude h_0 with a constant velocity V, the operating point flight path angle γ_0 is zero and hence the operating point pitch angle θ_0 and angle of attack α_0 are equal (but not zero). The range r thus varies linearly with time, i.e., r=Vt, since the horizontal velocity is V and the vertical velocity is zero. Under the above condition, the values of β_0, θ_0, K_{r0}, T_{r0} can be determined by solving the operating point equations along the horizontal

flight path, as shown in Equation (A.3) in Appendix I. The corresponding a and b parameters of the state space model, i.e. Equation (2-2), are thus determined.

The values β_0, θ_0, K_{r0} & T_{r0} at the operating point are found by solving Equation (A.3) in Appendix I. β_0, θ_0, K_{r0} & T_{r0} are functions of the flight condition, i.e., h, V & m. Since the a and b parameters of Equation (2-2) are functions of β_0, θ_0, K_{r0} & T_{r0}, see Equation (A.5), then the a and b parameters are functions of the flight condition (h,V,m).

2.1.3 The Transfer function of the System

The stability of the pitch axis system is determined by the pitch axis characteristic equation which can be found from its transfer function $H(s)=\delta X_3(s)/\delta u(s)$. In Laplace transform form Equation (2-2) becomes:

$$\begin{cases} s\cdot\delta x_1(s) = \delta x_2(s); \\ s\cdot\delta x_2(s) = \delta x_3(s)\cdot a_{23} + \delta x_4(s)\cdot a_{24} + \delta x_5(s)\cdot a_{25} + \delta u(s)\cdot b_2; \\ s\cdot\delta x_3(s) = \delta x_4(s); \\ s\cdot\delta x_4(s) = \delta x_3(s)\cdot a_{43} + \delta x_4(s)\cdot a_{44} + \delta x_5(s)\cdot a_{45} + \delta u(s)\cdot b_4; \\ s\cdot\delta x_5(s) = \delta x_6(s); \\ s\cdot\delta x_6(s) = \delta x_3(s)\cdot a_{63} + \delta x_4(s)\cdot a_{64} + \delta x_5(s)\cdot a_{65} + \delta x_6(s)\cdot a_{66} + \delta u(s)\cdot b_6; \end{cases} \tag{2-3}$$

It is usually a tedious task to solve Equation (2.3) for H(s). One straight-forward way of solving Equation (2.3) for H(s) is using the signal flow graph. The detailed procedure is referred to Appendix II.

As shown in Appendix II, the transfer function of the pitch axis system is:

$$H(s) = \frac{\delta x_3(s)}{\delta u(s)}$$

$$= \frac{b_4 s^2 - b_4 a_{66} s + a_{45} b_6 - a_{65} b_4}{s^4 - (a_{44} + a_{66}) s^3 + (a_{44} a_{66} - a_{65} - a_{43}) s^2 + (a_{65} a_{44} + a_{66} a_{43} - a_{45} a_{64}) s + a_{65} a_{43} - a_{63} a_{45}} \quad (2\text{-}4)$$

The pitch axis characteristic equation is,

$$W(s) = s^4 - (a_{44} + a_{66}) s^3 + (a_{44} a_{66} - a_{65} - a_{43}) s^2 + (a_{65} a_{44} + a_{66} a_{43} - a_{45} a_{64}) s + a_{65} a_{43} - a_{63} a_{45}.$$

The parameters of the transfer function H(s) as shown in Equation (2-4), are functions of the "a" and "b" parameters, and, as discussed in Section 2.1.2 of the Chapter 2, the "a" and "b" parameters are functions of the flight condition (V,h,m). So, the parameters of the transfer function H(s) vary with the speed(V), altitude (h), and mass (m). The stability and transient response of the pitch axis systems thus vary from one flight condition to another. Further details are discussed in Section 3.2.3 of Chapter 3.

2.2 The Desired Behavior of the System

The autopilot is assumed to be activated when level flight has been achieved after take-off. It then tracks the altitude command. The desired flight altitude is the reference signal input to the computer which can

vary with time. The desired closed-loop transfer function should not only stabilize the system but also maintain the required transient response within the desired flight envelope. The requirements for this study are, as suggested by Professor Saugen,

for an altitude command change of 100 feet,

(1) The rise time is between 5-12 second;

(2) The overshoot must be limited to 5%;

(3) The maximum acceleration is less than 0.8g .

The adaptive autopilot is required to modify system parameters so that the above requirements are met for any operating condition within the aircraft's specified flight regime .

CHAPTER 3

SYSTEM ANALYSIS AND COMPENSATION

As discussed in Chapter 1, selection of the adaptive control algorithm depends greatly on the system nature. This chapter discusses

1. pitch axis stability and compensation, and
2. examination of the system nonminimum phase nature.

3.1 Pitch Axis Stability and Compensation

Pitch axis stability for the uncompensated system during level flight can be determined from the root-locus plots of H(s) in Equation (2.4), as shown in Figure 3.1(a) through (c). The root-loci are greatly affected by the speed and the altitude variations which occur for the given flight envelop. There is always a root locus in the right half s-plane indicating that the system is **unstable over the entire desired flight envelope.** The design approach for the adaptive pitch axis autopilot assumes the adaptive autopilot is activated when the aircraft is in level flight. Since the uncompensated pitch axis system during level flight is unstable, it is appropriate to stabilize the aircraft using a compensator. A linear feedback loop is designed to stabilize the aircraft system during level flight within the entire desired flight envelope using methods present in Blakelock [1965] and Saugen [1987].

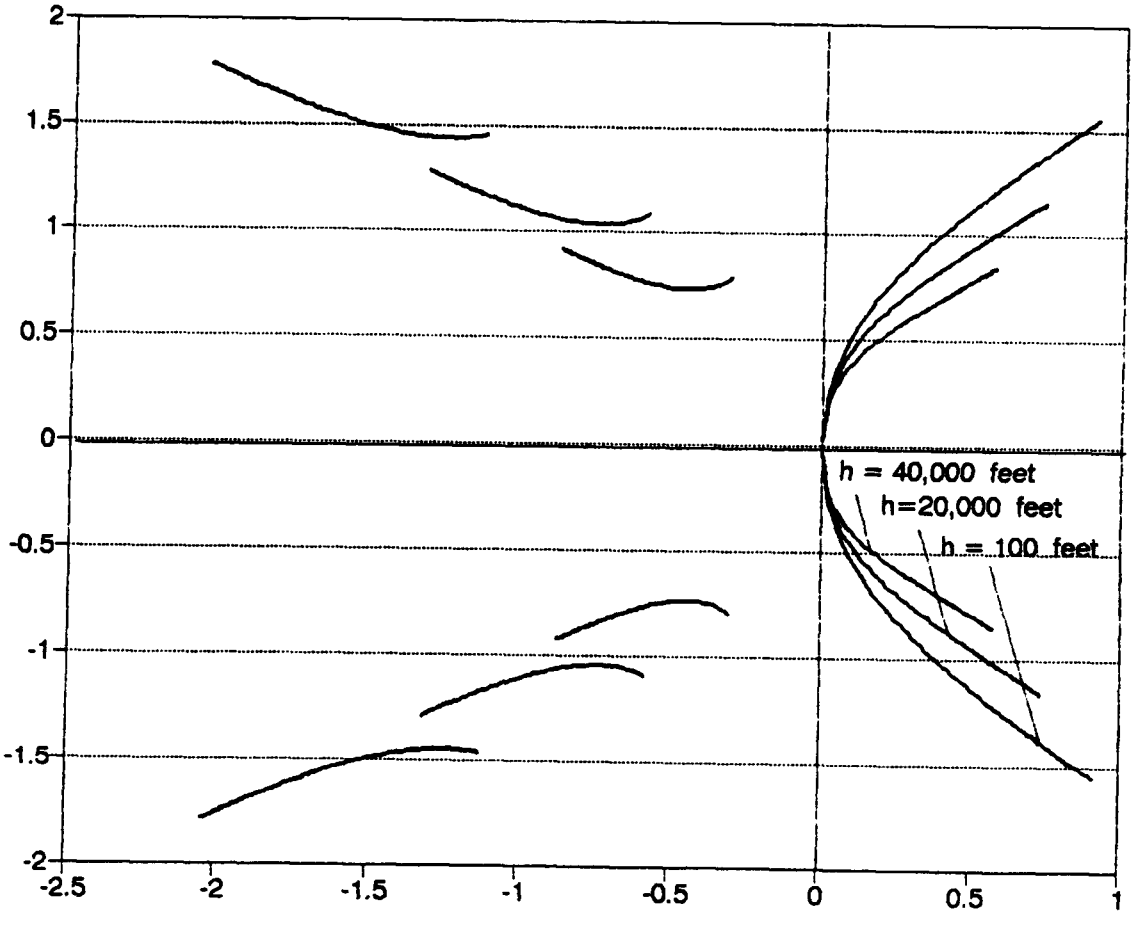

Figure 3.1(a) Root-Locus Altitude Variation for the Unstable Pitch Axis System. V=0.5 Mach; h=100, 20000, 40000 feet; W=10,000 Pound;

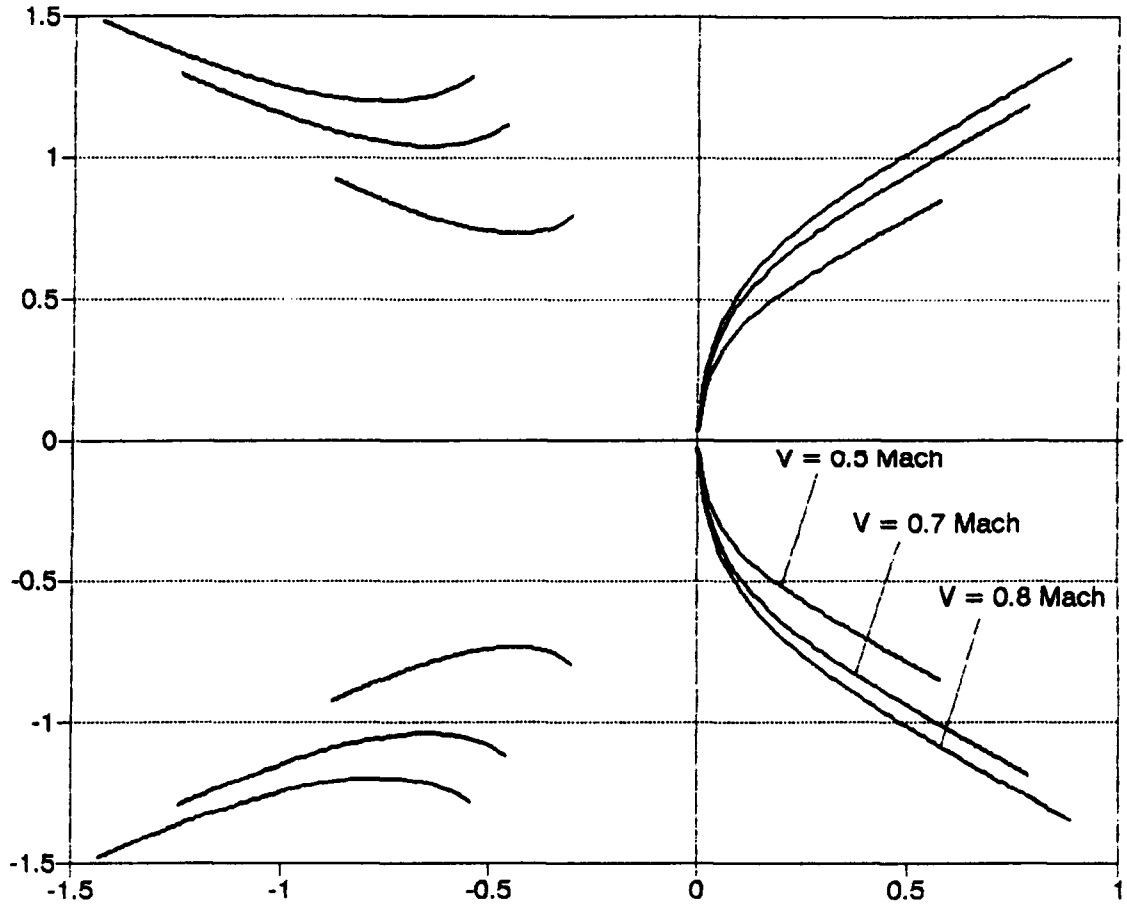

Figure 3.1(b) Root-Locus Speed Variation for the Unstable Pitch Axis System. V=0.5, 0.7, 0.8 Mach; h=40,000 feet; W=10,000 Pound.

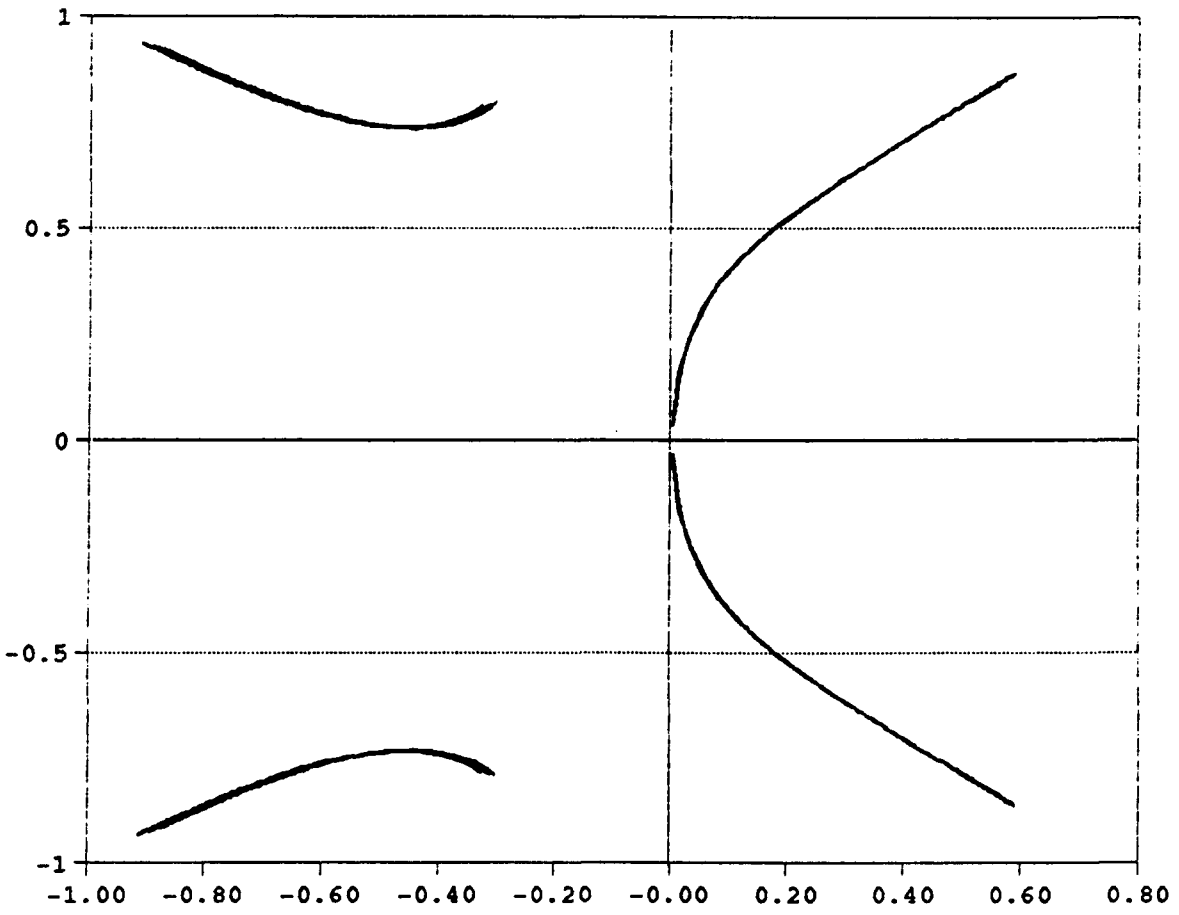

Figure 3.1(c) Root-Locus Weight Variation for the Unstable Pitch Axis System. W=10000, 9500, 9000 Pound; V=0.5 Mach; h=40,000 feet;

To stabilize the system, a compensator must be designed such that the right half s-plane root loci can be forced back to the left half s-plane. A rate-feedback compensator is found to be effective in meeting this goal. The rate-feedback compensator is discussed in the next section.

3.1.1 The Rate-Feedback Configuration

Figure 3.2 shows the system with rate-feedback as used by the analog controller. The rate-feedback is assumed perfect in this study. The system time response of the rate-feedback compensated system depends on the loop-gains K and K_t . The root-locus technique is used to determine the values for K and K_t which stabilize the pitch axis system for all level flight conditions within the desired flight envelope. Although the system is stable, desired behavior is not achieved for all flight conditions.

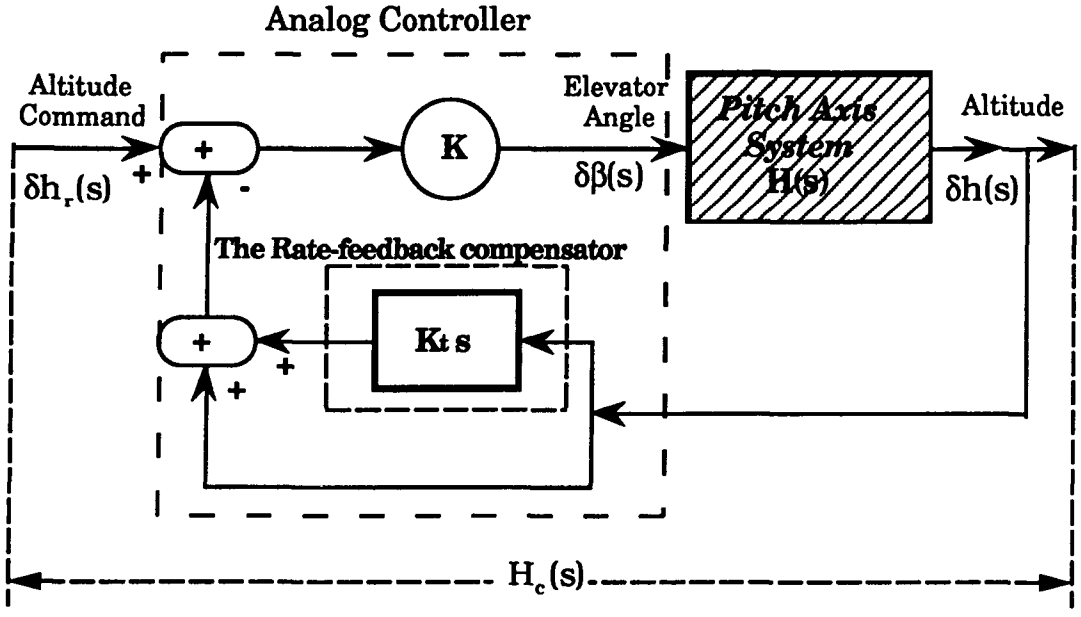

Figure 3.2 The Rate-feedback Pitch Axis System Forming the Analog Controller.

3.1.2 Determination of the Gains K and Kt

Figures 3.1 (a) and (b) show that the root-locus is closest to the real axis for low speeds and high altitudes. The root loci move toward the real axis as the dynamic pressure decreases. Root loci closer to the positive real axis are more difficult to compensate, i.e., to attract to the left-half s-plane. Hence, it is more difficult to stabilize the aircraft at low speeds and high altitudes. Consequently the following is hypothesized: A compensator designed to stabilize the pitch axis system for the lowest speed and the highest altitude within a desired flight envelope is stable for the entire flight envelope during level flight. This hypothesis is verified in Section 3.1.3.

The lowest speed and the highest altitude of the desired flight envelope is V=0.5 Mach and h=40,000 feet. Since the variation of the weight of the aircraft does not affect the root-locus of the system significantly, as shown in Figure 3.1(c), the weight corresponding to the flight condition for the design of the compensator is thus taken as the initial weight of the system, i.e., w=10,000 pounds. The transfer function corresponding to V=0.5 Mach, h=40,000 feet & w=10,000 pounds is thus used in the design of K and Kt. The operating point condition under the flight condition is given by Equation (A.3) of Appendix I, that is: θ_0=7.39 degree; β_0=3.70 degree; T_{r0} (trust)=22,955 pound. The transfer function at the operating point is:

$$H(s) = \frac{\delta h(s)}{\delta \beta(s)} = \frac{(-2.197\, s^2 - 0.03165\, s + 5.6743)\cdot 1000}{s^4 + 0.5951\, s^3 + 0.7175\, s^2 - 0.00462\, s + 0.0006758} \quad (3\text{-}1)$$

where δh is expressed in feet and $\delta\beta$ is in degree.

The closed-loop transfer function of the compensated pitch axis system, as shown in Figure 3.2 can be expressed as,

$$H_c(s) = \frac{\delta h(s)}{\delta h_r(s)} = \frac{K\, H(s)}{1 + K\, H(s)\cdot(K_t\, s + 1)} \quad (3\text{-}2)$$

where δh and δh_r are expressed in feet;

δh_r is the reference altitude command.

As shown in Equation (3-2), the poles of the rate-feedback compensated system are the zeros of $1 + K\, H(s)\cdot(K_t\, s + 1)$. The stability of the rate feedback compensated system depends on the gains K and K_t of the feedforward loop and the feedback loop, respectively.

Root-locus plots for $1 + K\, H(s)\cdot(K_t\, s + 1)$ are generated by first assigning a constant value to K_t and then K is allowed to vary for K>0. The root-locus plots for K_t =0.5, 0.7, and 1.2 are shown in Figure 3.3 (b) with K varying from 0 to 0.3. The four loci are symmetrical with respect to the horizontal axis. The open-loop poles of H(s) in Equation (3-1) are $p_{1,2}$=0.0036±j0.0305 and $p_{3,4}$=-0.3011±j0.7939. Note that $p_{1,2}$ are unstable poles.

For K_t =0.5 or 0.7 Figure 3.3 (b) shows that the right half plane root loci remains in the right-half s-plane, implying the rate-feedback

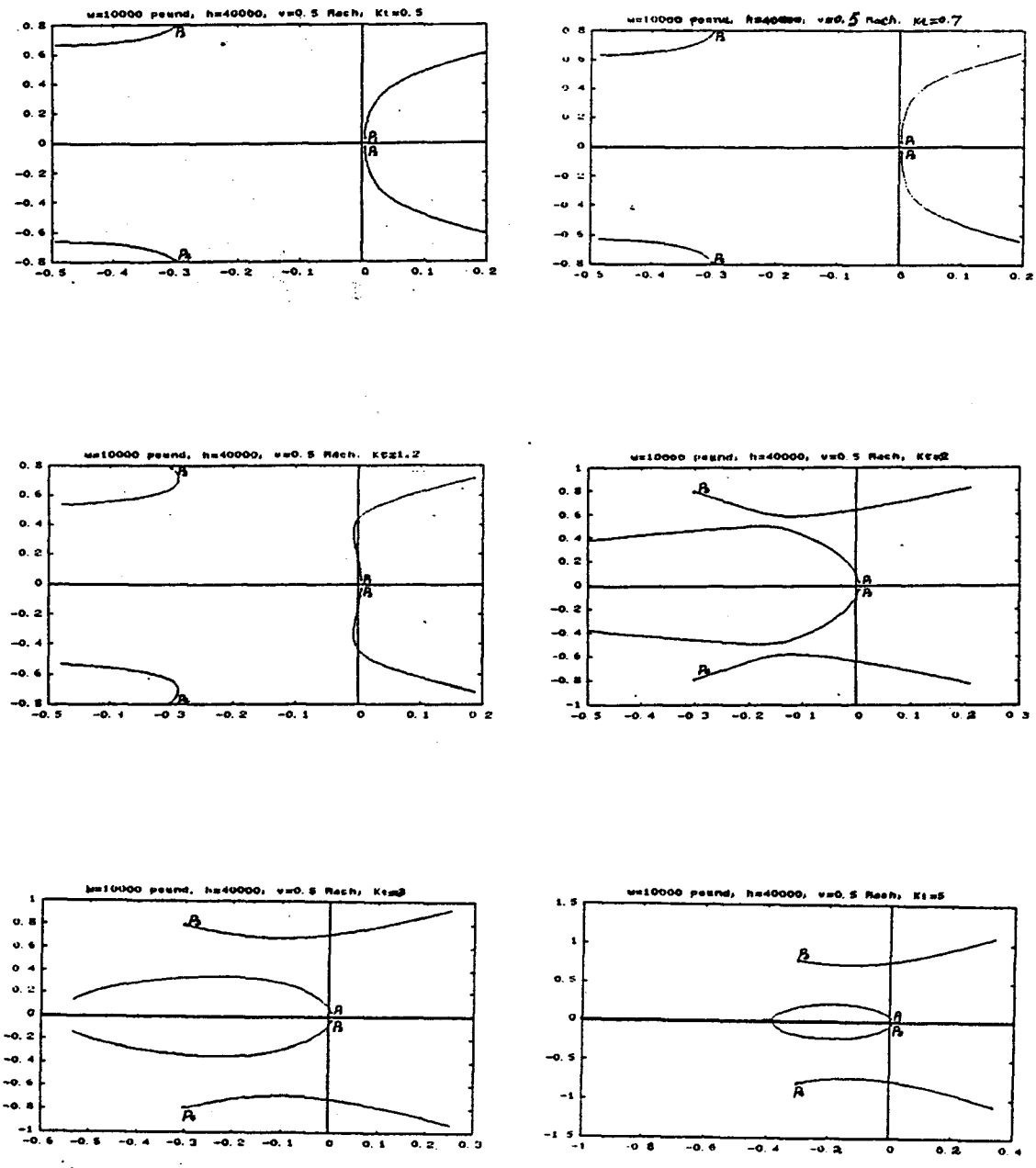

Figure 3.3(a) Rate-Feedback Pitch Axis System Root-Loci As Kt Changes.

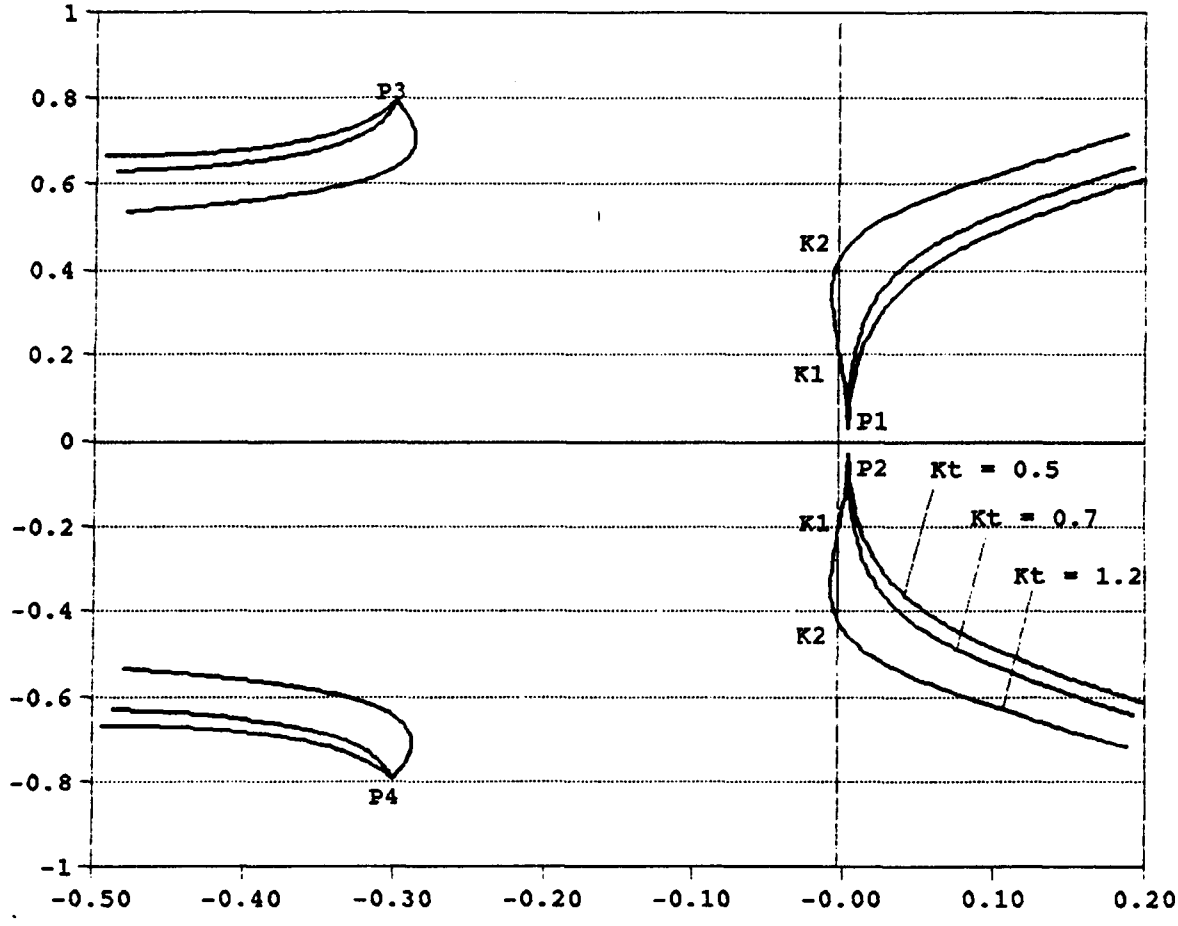

Figure 3.3(b) Rate-Feedback Pitch Axis System Root-Loci.
W=10,000 Pound; V=0.5 Mach; h=40,000 feet.
Kt=0.5, 0.7, 1.2;

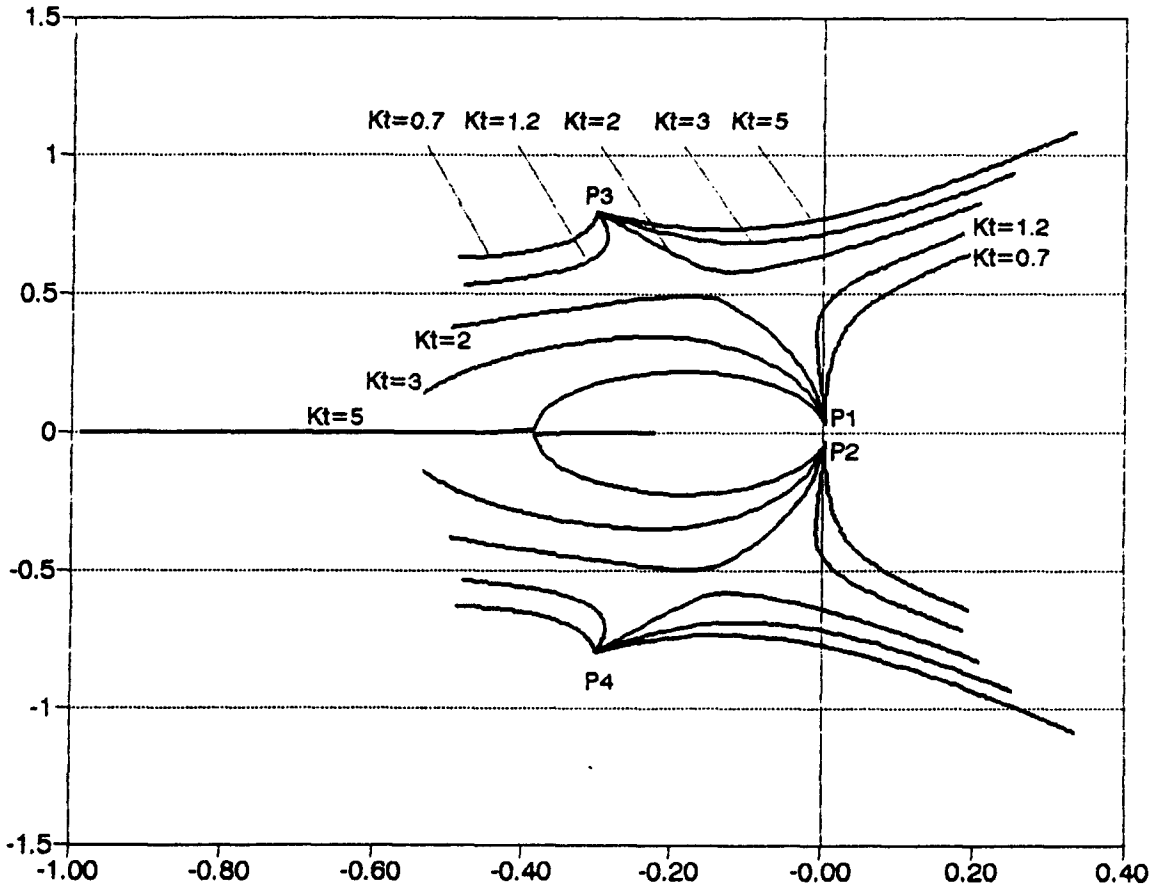

Figure 3.3(c) Rate-feedback Pitch Axis System Root-Loci.
W=10,000 Pound; V=0.5 Mach; h=40,000 feet.
Kt=0.7, 1.2, 2, 3, 5;

compensated system is always unstable for K_t =0.5 or 0.7. For K_t =1.2, a portion of the root-locus departing from p_1 and p_2 is in the left half s-plane. For this value of K_t , a gain K can be selected to stabilize the system, where $K_1<K<K_2$ as indicated in Figure 3.3 (b). However K_t =1.2 might not be a good choice since a very lightly damped system results for all values of K between K_1 and K_2. If K_t is chosen such that K_1 and K_2 are very close, the selections of K is very restricted and small errors in gain K lead to an unstable system.

As shown in Figure 3.3 (c), the root loci starting at p_3 and p_4 for $K_t>K_{critical}$ cross the imaginary axis and never return to the left half plane for 0<K<0.05. Note, $K_{critical}$ is the value of K_t at which the root-loci starts to cross the imaginary axis, as indicated in Figure 3.4. At the same time, root loci departing from p_1 and p_2 enter the left-half s-plane and never return to the right-half plane. The root-loci always intercept the imaginary axis at four points.

The root-locus plots of Figure 3.3 (b) and Figure 3.3 (c) show that the range of K for stable operation depends on K_t. The relationship between K and K_t for stable operation is shown in Figure 3.4. Mathematical derivations and simulations of the relationship between K and K_t are as shown in the following.

If the root-locus intercepts the imaginary axis at jω, then, s=jω is a root of $1+K\,H(s)\cdot(K_t\,s+1)$, i.e.,

$$1+K\,H(s)\cdot(K_t\,s+1)=0.$$

Let,

$$H(s) = \frac{\mu_2 s^2 + \mu_1 s + \mu_0}{s^4 + \vartheta_3 s^3 + \vartheta_2 s^2 + \vartheta_1 s + \vartheta_0}$$

then,

$$K = \frac{-1}{H(j\omega)(K_t\ j\omega + 1)}$$

$$= \frac{-1}{(K_t\ j\omega + 1)\ \dfrac{(-\mu_2\omega^2 + \mu_1 j\omega + \mu_0)}{\omega^4 - \vartheta_3\omega^3 j - \vartheta_2\omega^2 + \vartheta_1\omega j + \vartheta_0}}$$

$$= \frac{RL + j\,IM}{(\mu_0 - \mu_1 K_t\omega^2 - \mu_2\omega^2)^2 + (\mu_0 K_t\omega + \mu_1\omega - \mu_2 K_t\omega^3)^2} \qquad (3\text{-}3)$$

where,

$$RL = -[(\omega^4 - \vartheta_2\omega^2 + \vartheta_0)(\mu_0 - \mu_1 K_t\omega^2 - \mu_2\omega^2) + (\vartheta_1\omega - \vartheta_3\omega^3)(\mu_0 K_t\omega + \mu_1\omega - \mu_2 K_t\omega^3)] \qquad (3\text{-}4)$$

$$\begin{aligned} IM &= -[(\vartheta_1\omega - \vartheta_3\omega^3)(\mu_0 - \mu_1 K_t\omega^2 - \mu_2\omega^2) - (\omega^4 - \vartheta_2\omega^2 + \vartheta_0)(\mu_0 K_t\omega + \mu_1\omega - \mu_2 K_t\omega^3)] \\ &= \omega \cdot [(-\mu_2 K_t)\omega^6 + (\mu_1 + \mu_2\vartheta_2 K_t - \mu_1\vartheta_3 K_t - \mu_2\vartheta_3 + \mu_0 K_t)\omega^4 \\ &\quad + (\mu_0\vartheta_3 + \mu_1\vartheta_1 K_t + \mu_2\vartheta_1 - \mu_0\vartheta_2 K_t - \mu_1\vartheta_2 - \mu_2\vartheta_0 K_t)\omega^2 \\ &\quad + (\mu_1\vartheta_0 + \mu_0\vartheta_0 K_t - \mu_0\vartheta_1)] \end{aligned} \qquad (3\text{-}5)$$

Since gain k is real, the imaginary part of (3-4) is thus zero, i.e.,

$$(-\mu_2 K_t)\omega^6 + (\mu_1 + \mu_2\vartheta_2 K_t - \mu_1\vartheta_3 K_t - \mu_2\vartheta_3 + \mu_0 K_t)\omega^4 + (\mu_0\vartheta_3 + \mu_1\vartheta_1 K_t + \mu_2\vartheta_1 - \mu_0\vartheta_2 K_t - \mu_1\vartheta_2 - \mu_2\vartheta_0 K_t)\omega^2 + (\mu_1\vartheta_0 + \mu_0\vartheta_0 K_t - \mu_0\vartheta_1) = 0 \qquad (3\text{-}6a)$$

So,
$$K = \frac{RL}{(\mu_0 - \mu_1 K_t\omega^2 - \mu_2\omega^2)^2 + (\mu_0 K_t\omega + \mu_1\omega - \mu_2 K_t\omega^3)^2} \qquad (3\text{-}6b)$$

Therefore, if K_t is known, the roots (ω) of Equation (3-6a) can be determined and then gain K can be found from Equation (3-6b). Figure 3.3(b) shows that the root-loci starts to cross the imaginary axis when K_t is around 1. The simulation of K_t varies from 0 to 10 is shown in Figure 3.4.

As shown in Figure 3.4, the range of K for stable operation is the greatest when K_t is approximately 2. Any value of K and K_t within the shaded area can be chosen to stabilize the system. It is not necessary to choose K_t such that K has the largest range. However, choosing K for the largest range of values of K for stable operation results in the most robust system. So, K=0.015 and K_t =2 are chosen for the design.

For V=0.5 Mach, h=40,000 feet, m=10,000 pound, K=0.015, & K_t =2, the rate-feedback compensated system transfer function in Equation (3-2) becomes,

$$H_c(s) = \frac{-0.032999\,s^2 - 0.00047485\,s + 0.08511}{s^4 + 0.58848\,s^3 + 0.73253\,s^2 + 0.16513\,s + 0.085793} \qquad (3\text{-}10)$$

3.1.3 Verifications of the Rate-Feedback Compensated System

Figure 3.5 shows the stable region for the rate-feedback compensated pitch axis system at level flight with K=0.015 and K_t=2. The

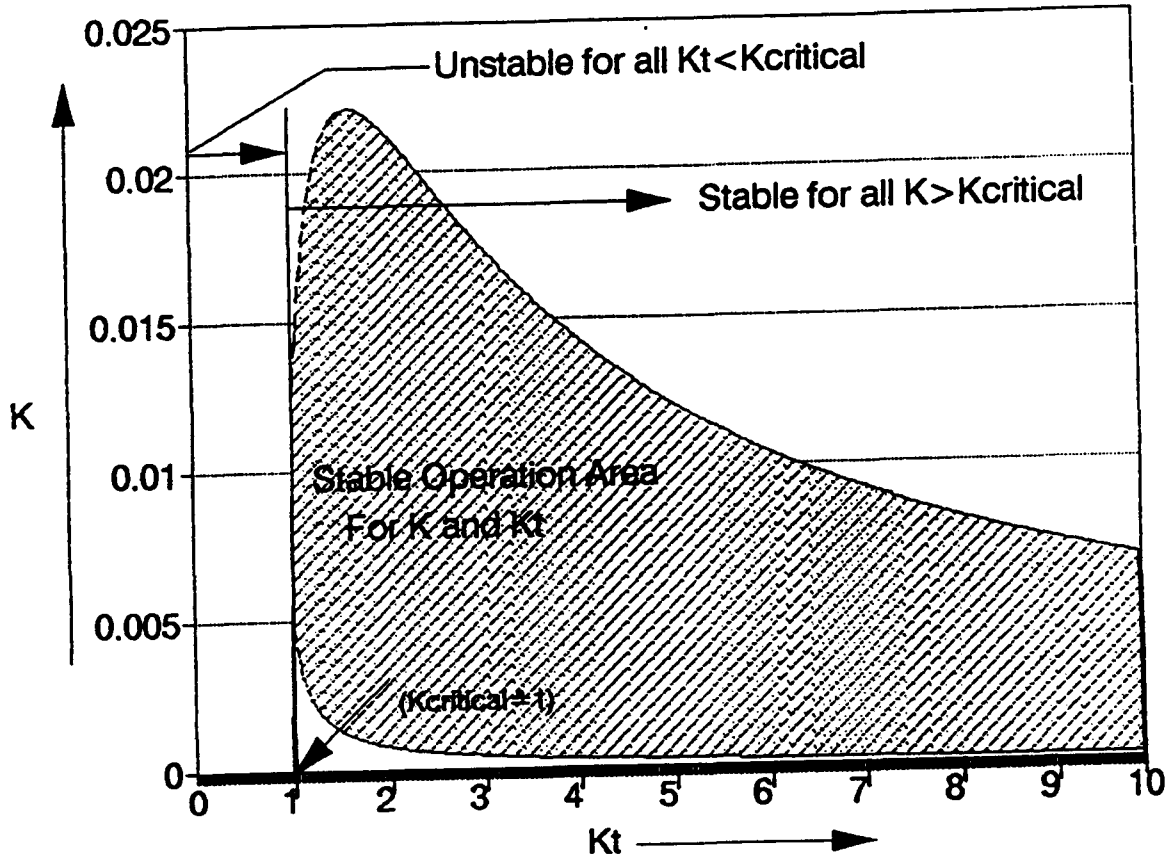

Figure 3.4 Stable Operation Area For Selection of K and Kt.

stability region is plotted based on the information of the unstable zero(s) of $1+K\,H(s)\cdot(K_t\,s+1)$ within the speed varying from 0.2 Mach to 0.85 Mach. The stable altitude corresponding to each speed increases from zero feet until an unstable zero of $1+K\,H(s)\cdot(K_t\,s+1)$ is detected.

As shown in Figure 3.5, the desired flight envelope is well covered by the stability region. So, the pitch axis system at level flight is stabilized by the rate-feedback compensator with K=0.015 and K_t=2.

The rate-feedback compensator is applied to stabilize the system only, it does not guarantee the transient response of the system meets specifications. In fact, the transient response of the rate-feedback pitch axis system varies from one flight condition to another.

Figures 3.6 (a) through (d) show the transient responses and vertical accelerations of the rate-feedback pitch axis system for some particular level flight conditions. Figures 3.6 (a) & (b) show the transient responses and vertical accelerations corresponding to the specified speeds and an unchanging altitude while Figures 3.6 (c) & (d) show those of the specified altitude and an unchanging speed. As shown in Figure 3.6(a) & (b), the maximum percentage overshoot of V=0.5 Mach is greater than that for V=0.8 Mach but the maximum vertical acceleration of V=0.5 Mach is less than that for V=0.8 Mach. Note that in Figure 3.6(a) the maximum percentage overshoots are greater than 15% and in Figure 3.6 (b) the maximum vertical acceleration is about 28 feet/sec^2 which is greater than 0.8g. Furthermore, the percentage overshoot decreases as the speed increases and the maximum vertical acceleration increases as

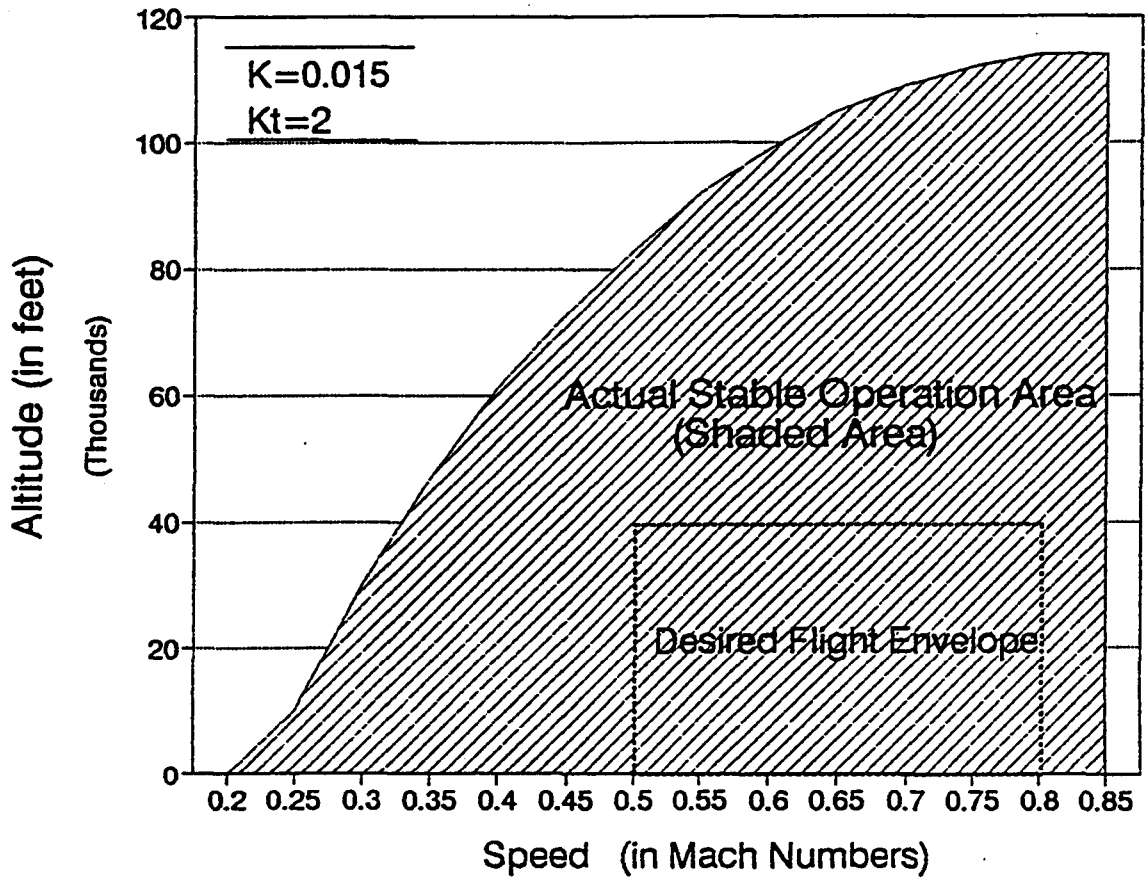

Figure 3.5 Rate-Feedback Pitch Axis System Stable Flight Envelope.

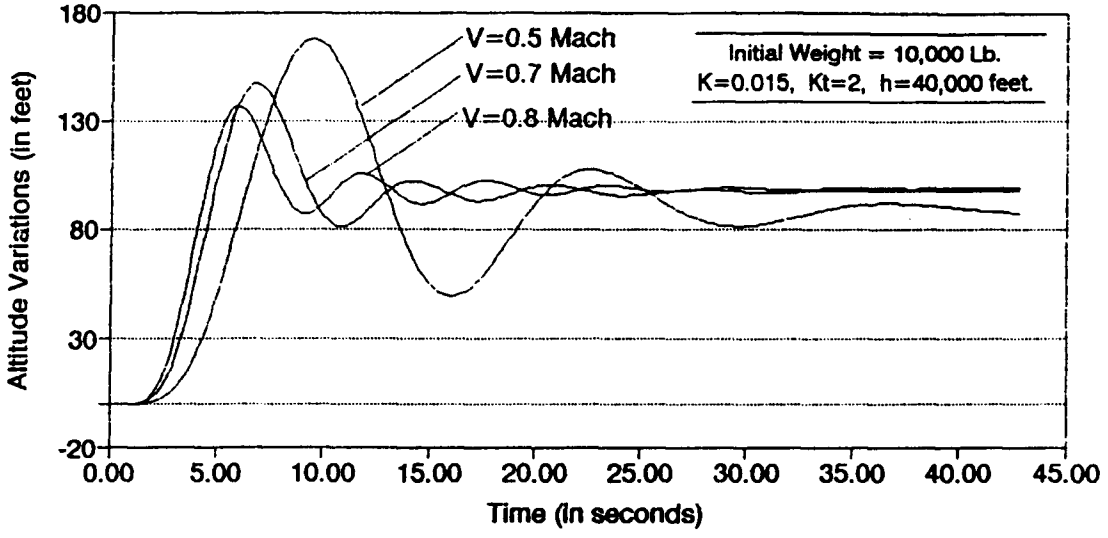

Figure 3.6(a) Level Flight Rate-Feedback Pitch Axis System Step Response. W=10,000 Pound; V=0.5, 0.7, 0.8 Mach; h=40,000 feet.

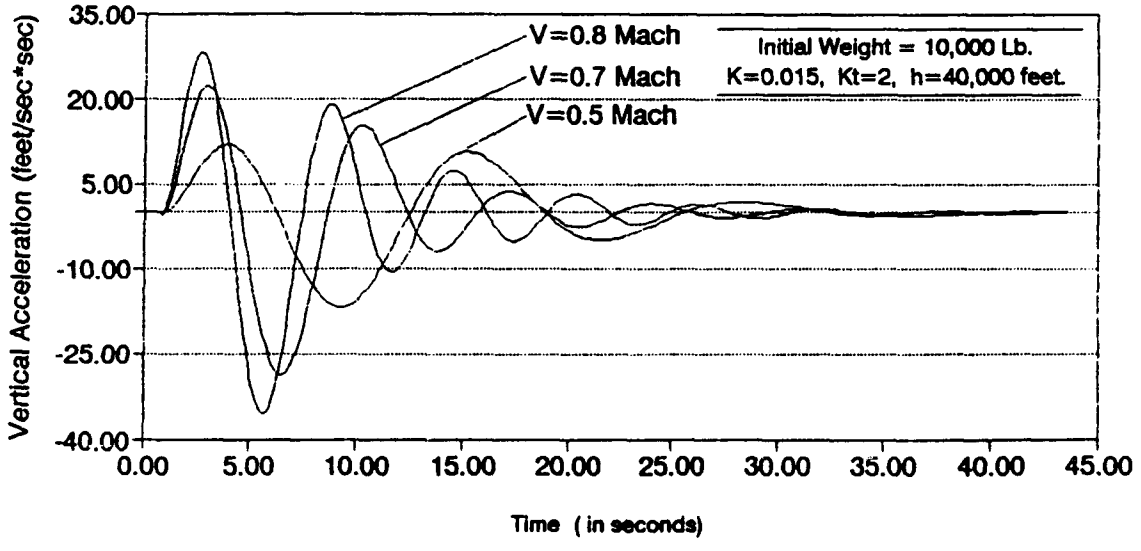

Figure 3.6(b) Vertical Acceleration to the 100 feet Command Change. W=10,000 Pound; V=0.5, 0.7, 0.8 Mach; h=40,000 feet.

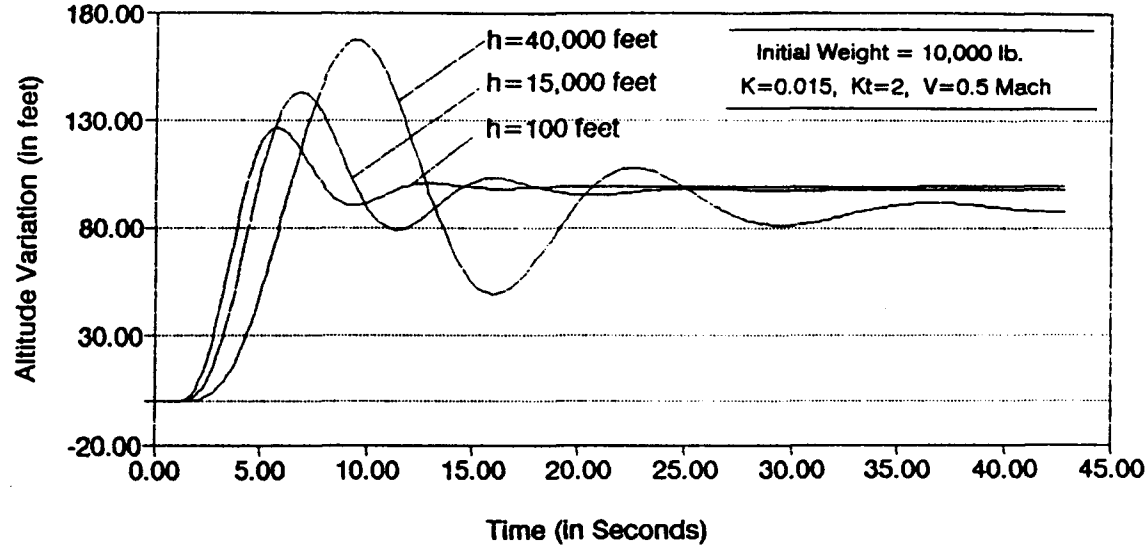

Figure 3.6(c) Level Flight Rate-Feedback Pitch Axis System Step Response. W=10,000 Pound; h=40000, 15000, 100 feet; V=0.5 Mach.

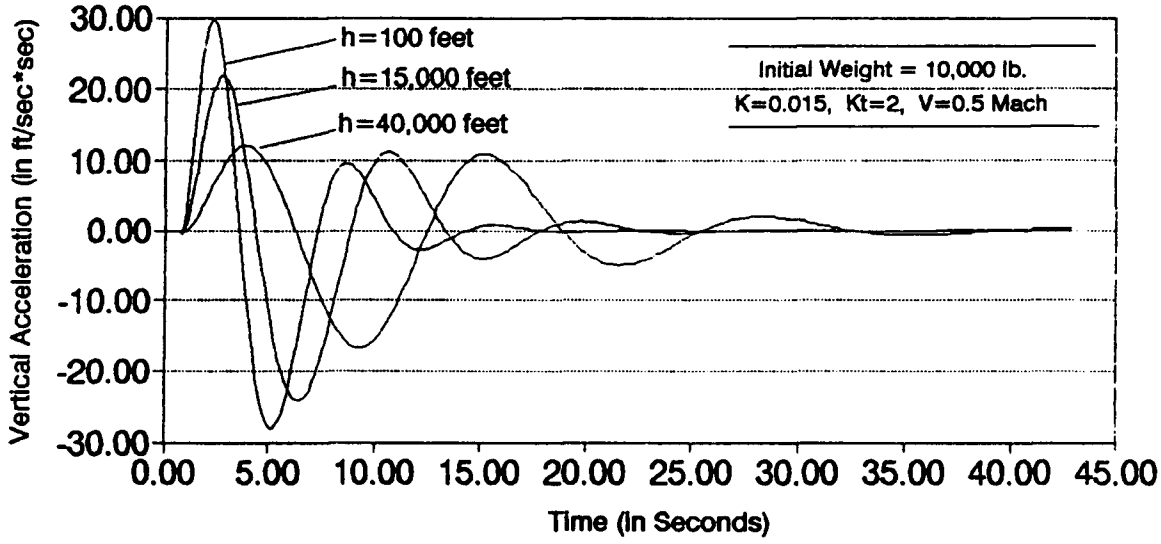

Figure 3.6(d) Vertical Acceleration to the 100 feet Command Change. W=10,000 Pound; V=0.5 Mach; h=40000, 15000, 100 feet.

the speed decreases . Similar variations in transient response are also observed in Figure 3.6 (b). Note that Figures (a) through (d) are plotted based on nonlinear simulations of the rate-feedback pitch axis system shown in Figure 3.2. Details on the simulations are referred to Section 5.1.

3.2 Examination of the System Nonminimum Phase Nature

The level flight pitch axis transfer function is, as shown in Equation (2-4),

$$H(s) = \frac{b_4 s^2 - b_4 a_{66} s + a_{45} b_6 - a_{65} b_4}{s^4 - (a_{44} + a_{66}) s^3 + (a_{44} a_{66} - a_{65} - a_{43}) s^2 + (a_{65} a_{44} + a_{66} a_{43} - a_{45} a_{64}) s + a_{65} a_{43} - a_{63} a_{45}}.$$

The numerator polynomial of the transfer function is b_4s^2-$a_{66}b_4s$+$a_{45}b_6$-$a_{65}b_4$. The zeros are thus the roots of $N(s) = s^2$-$a_{66}s$+($a_{45}b_6/b_4$-a_{65}).

The parameters b_4, b_6, a_{45}, and a_{65}, as shown in Equation (A. 5), are

$$\begin{cases} b_4 = -DPM \cdot c_{l\beta} = -\dfrac{DP}{m} \cdot c_{l\beta} \\ b_6 = -DPJ \cdot c_{l\beta} = -\dfrac{DP}{J} \cdot r_e c_{l\beta} \\ a_{45} = \dfrac{T}{m} + DPM\left(c_{l\alpha} - c_{d\alpha} - c_{d\beta}\right) = \dfrac{T}{m} + \dfrac{DP}{M}\left(c_{l\alpha} - c_{d\alpha} - c_{d\beta}\right) \\ a_{65} = -DPJ \cdot r_{cp} c_{l\alpha} = -\dfrac{DP}{m} \cdot r_{cp} c_{l\alpha} \end{cases}$$

where, $DP = \frac{1}{2}\rho V^2$ with $\rho = \rho_z\, e^{-\frac{h_0}{H}}$;

ρ_z, H, $c_{l\alpha}$, $c_{l\beta}$, $c_{d\alpha}$, $c_{d\beta}$, $c_{m\theta}$, and J are aerodynamic coefficients given in Table 2.1.

T is the thrust of the aircraft, which is positive;

r_{cp}=0.5 feet and r_e=20 feet as provided in Section 2.1.

So,

$$
\begin{aligned}
& a_{45}b_6 / b_4 - a_{65} \\
&= \left[\frac{T}{m} + \frac{DP}{m}\left(c_{l\alpha} - c_{d\alpha} - c_{d\beta}\right)\right] \cdot \left(\frac{DP}{J} r_e c_{l\beta}\right) \Big/ \left(-\frac{DP}{m} c_{l\beta}\right) - \left(-\frac{DP}{J} r_{cp} c_{l\alpha}\right) \\
&= \left[\frac{T}{m} + \frac{DP}{m}\left(c_{l\alpha} - c_{d\alpha} - c_{d\beta}\right)\right] \cdot \left(-\frac{m}{J} r_e\right) - \left(-\frac{DP}{J} r_{cp} c_{l\alpha}\right) \\
&= -\left[\frac{T}{J} r_e + \frac{DP}{J}\left(r_e c_{l\alpha} - r_e c_{l\alpha} - r_e c_{d\beta}\right)\right] - \left(-\frac{DP}{J} r_{cp} c_{l\alpha}\right) \\
&= -\left[\frac{T}{J} r_e + \frac{DP}{J}\left(r_e c_{l\alpha} - r_e c_{l\alpha} - r_e c_{d\beta} - r_{cp} c_{l\alpha}\right)\right] \\
&= -\left[\frac{T}{J} r_e + \frac{\rho V^2}{2J}(20 \times 13.96 - 20 \times 10 - 20 \times 0.5 - 0.5 \times 13.96)\right] \\
&= -\left[\frac{T}{J} r_e + \frac{\rho V^2}{2J}(62.22)\right] < 0
\end{aligned}
$$

The constant term of N(s), i.e., $(a_{45}b_6/b_4-a_{65})$, is negative implies that the product of the roots of the N(s) is negative. Therefore, N(s) has a positive root and a negative root. The level flight pitch axis system is thus a nonminimum phase system for the entire flight envelope.

The rate-feedback pitch axis transfer function during level flight is, as shown in Equation (3-2),

$$
H_c(s) = \frac{\delta h(s)}{\delta h_r(s)} = \frac{K\,H(s)}{1 + K\,H(s) \cdot (K_t\,s + 1)} \quad .
$$

Since the transfer function of the level flight pitch axis system, i.e., H(s), always has a zero on the right half s-plane, the rate-feedback level flight pitch axis system is also a nonminimum phase system for the entire desired flight envelope.

CHAPTER 4

ADAPTIVE CONTROL LOOP DESIGN

The pitch axis autopilot system configuration is shown in Figure 1.1. The system is composed of an inner loop and an outer loop. The inner loop consists of the controller and the aircraft dynamics which determines the transfer function of the closed-loop system. The design of the inner loop is the controller design. The outer loop consists of a parameter estimator and adaptive process algorithm. The parameter estimator estimates the parameters of the aircraft system using the sampled data of the input and output of the aircraft system. The parameters of the controller in the inner loop are adjusted every sample-period using the results of the adaptive process algorithm.

4.1 Selection of the Adaptive Control Algorithm

As discussed in Section 3.2 of Chapter 3, the pitch axis system of the aircraft at level flight is a nonminimum phase system for the entire flight envelope. As it is discussed in Clark [1984], the use of common algorithms such as MRAC and early self-turning regulators can cause instability of the closed-loop system.

Pole-placement algorithms are discussed in many papers, such as Astrom & Wittenmark [1980] [1984] and Goodwin & Sin [1981] [1984]. Together with theoretical derivations, proofs and simulations, these

papers show that the pole-placement algorithm can be used effectively for adaptive control of deterministic time-invariant nonminimum phase systems. The structures of the pole-placement algorithms in Astrom & Wittenmark [1980] [1984] and Goodwin & Sin [1981] [1984] are actually the same except that the error driven feedback controller is used in Goodwin & Sin [1981][1984] while the general feedback controller is used in Astrom & Wittenmark[1980][1984]. The convergence of the pole-placement algorithm is proven in Goodwin & Sin [1981][1984]. The deterministic servo design is seriously considered in Astrom & Wittenmark [1980][1984]. Since the requirement for the adaptive pitch axis autopilot is to maintain the desired transient response of the aircraft system, the design approach here is based on the pole-placement algorithm proposed in Astrom & Wittenmark [1980]. Steady-state tracking error minimization is also presented.

4.2 Design of the Inner Loop Using the Pole-placement Algorithm

4.2.1 The Plant z-transfor Model

The adaptive pitch axis autopilot is assumed to be implemented digitally. The sampled data pitch axis system is modeled using a zero-order-hold (ZOH) in the forward path of the system and sampling the output.

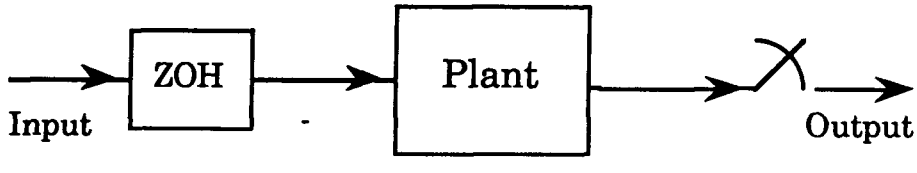

In general, the z-transfer function of a linear stationary dynamic system can be expressed as,

$$\frac{B(z)}{A(z)} = \frac{\beta_1 z^{-1} + \beta_2 z^{-2} ..... \beta_{n-1} z^{-(n-1)} + \beta_n z^{-n}}{1 + \alpha_1 z^{-1} + \alpha_2 z^{-2} ..... + \alpha_{n-1} z^{-(n-1)} + \alpha_n z^{-n}}$$

The pitch axis system transfer function in Equation (2-4) is a 4th order system. The order of the corresponding z-transfer function is thus 4. So, the degrees of polynomials A(z) and B(z) are less than or equal 4, that is,

$$A(z) = 1 + \hat{\alpha}_1 \cdot z^{-1} + \hat{\alpha}_2 \cdot z^{-2} + \hat{\alpha}_3 \cdot z^{-3} + \hat{\alpha}_4 \cdot z^{-4};$$
$$B(z) = \hat{\beta}_1 \cdot z^{-1} + \hat{\beta}_2 \cdot z^{-2} + \hat{\beta}_3 \cdot z^{-3} + \hat{\beta}_4 \cdot z^{-4}$$

where $\hat{\alpha}_1, \hat{\alpha}_2, \hat{\alpha}_3, \hat{\alpha}_4, \hat{\beta}_1, \hat{\beta}_2, \hat{\beta}_3, \hat{\beta}_4$ are the identified system parameters for each sampling period** .

The discrete time sampled-data pitch axis model is:

$$\begin{aligned} &y(t) + \hat{\alpha}_1\, y(t-T) + \hat{\alpha}_2\, y(t-2T) + \hat{\alpha}_3\, y(t-3T) + \hat{\alpha}_4\, y(t-4T) \\ &= \hat{\beta}_1\, u(t-T) + \hat{\beta}_2\, u(t-2T) + \hat{\beta}_3\, u(t-3T) + \hat{\beta}_4\, u(t-4T); \end{aligned} \qquad (4\text{-}1)$$

Hence,

$$A(z)y(z) = B(z)u(z)$$

where, y is the sampled-data output (altitude in feet);

u(t) is the calculated input signal the analog system (in feet);

T is the sampling time (in second);

t is the discrete time, i.e., t=kT, with k=1,2,3.....

** z^{-k} is utilized here as a delay operator of k sampling periods.

4.2.2 The Overall System

The adaptive controller utilizes the linear feedback regulator shown in Figure 4.1.

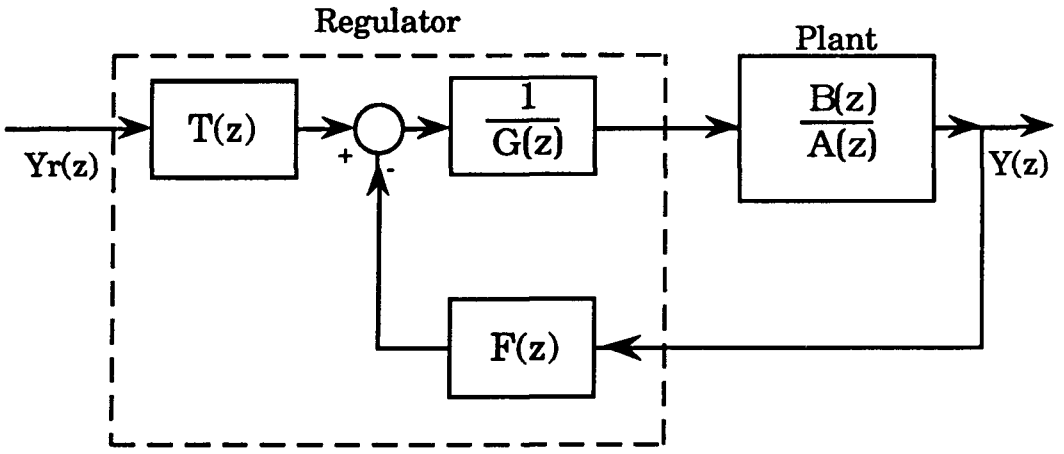

Figure 4.1 Linear Feedback Regulator Used by the Adaptive Controller.

T(z), F(z) and G(z) shown in Figure 4.1 are polynomials in the delay operator z^{-1} . The orders of T(z), F(z) and G(z) used for the design are given Section 4.3. Adaptive control is realized by adjusting the parameters of T(z), F(z) and G(z) in response to changes in the plant.

The closed-loop transfer function of the system is then given by

$$Y(z) = \frac{T(z)\,B(z)}{A(z)\,G(z) + B(z)\,F(z)}\,Y_r(z) \qquad (4\text{-}2)$$

The closed loop eigenvalues, i.e. the roots of the closed loop characteristic equation A(z)G(z)+B(z)F(z), can be "assigned" by proper choice of G(z) and F(z) in response to changes in A(z) and B(z). Thus the following equation must be solved,

$$A(z)G(z)+B(z)F(z)= A_m(z) \tag{4-3}$$

where $A_m(z)$ is the desired closed-loop characteristic equation.
Thus G(z) and F(z) are continuously modified by the adaptive process algorithm so that the closed loop eigenvalues are the same as the roots of $A_m(z)$.

4.3 Controller Parameter Calculations

4.3.1 Determination of F(z) and G(z)

The desired closed-loop poles are the roots of $A_m(z)$ at the desired locations, F(z) and G(z) must satisfy

$$A(z)G(z)+B(z)F(z) = A_m(z) \tag{4-4}$$

As discussed by Astrom & Wittenmark [1990], Equation (4-3) has infinitely many solutions. For example, if $F_0(z)$ and $G_0(z)$ are solutions, then, the following are solutions:

$$\begin{cases} G(z) = G_0(z) + B(z)W(z) \\ F(z) = F_0(z) - A(z)W(z) \end{cases} \tag{4-5}$$

where W(z) is an arbitrary scalar polynomial.

As shown in Appendix III, F(z) and G(z) are determined according to Theorem 5.3.1 of Goodwin & Sin [1984]. The procedure for solving Equation (4-3) follows.

As discussed in Section 4.2.1, the maximum degree of A(z) and B(z) is 4. According Theorem 5.3.1 of Goodwin & Sin [1984], the degrees for F(z) and G(z) are taken as 3 to have unique solution. The polynomials F(z) and G(z) can be expressed as,

$$\begin{cases} F(z) = f_0 + f_1 \cdot z^{-1} + f_2 \cdot z^{-2} + f_3 \cdot z^{-3} \\ G(z) = g_0 + g_1 \cdot z^{-1} + g_2 \cdot z^{-2} + g_3 \cdot z^{-3} \end{cases} \tag{4-6}$$

From Equation (4-3) it follow that the desired closed-loop characteristic Equation is 7th order, i.e.,

$$A_m(z) = \alpha_0^* + \alpha_1^* \cdot z^{-1} + \alpha_2^* \cdot z^{-2} + \alpha_3^* \cdot z^{-3} + \alpha_4^* \cdot z^{-4} + \alpha_5^* \cdot z^{-5} + \alpha_6^* \cdot z^{-6} + \alpha_7^* \cdot z^{-7}. \tag{4-7}$$

Equating coefficients of like power of z on both side of Equation (4-3) gives:

$$\begin{bmatrix} 1 & 0 & 0 & 0 & 0 & 0 & 0 & 0 \\ \hat{\alpha}_1 & 1 & 0 & 0 & \hat{\beta}_1 & 0 & 0 & 0 \\ \hat{\alpha}_2 & \hat{\alpha}_1 & 1 & 0 & \hat{\beta}_2 & \hat{\beta}_1 & 0 & 0 \\ \hat{\alpha}_3 & \hat{\alpha}_2 & \hat{\alpha}_1 & 1 & \hat{\beta}_3 & \hat{\beta}_2 & \hat{\beta}_1 & 0 \\ \hat{\alpha}_4 & \hat{\alpha}_3 & \hat{\alpha}_2 & \hat{\alpha}_1 & \hat{\beta}_4 & \hat{\beta}_3 & \hat{\beta}_2 & \hat{\beta}_1 \\ 0 & \hat{\alpha}_4 & \hat{\alpha}_3 & \hat{\alpha}_2 & 0 & \hat{\beta}_4 & \hat{\beta}_3 & \hat{\beta}_2 \\ 0 & 0 & \hat{\alpha}_4 & \hat{\alpha}_3 & 0 & 0 & \hat{\beta}_4 & \hat{\beta}_3 \\ 0 & 0 & 0 & \hat{\alpha}_4 & 0 & 0 & 0 & \hat{\beta}_4 \end{bmatrix} \begin{bmatrix} g_0 \\ g_1 \\ g_2 \\ g_3 \\ f_0 \\ f_1 \\ f_2 \\ f_3 \end{bmatrix} = \begin{bmatrix} \alpha_0^* \\ \alpha_1^* \\ \alpha_2^* \\ \alpha_3^* \\ \alpha_4^* \\ \alpha_5^* \\ \alpha_6^* \\ \alpha_7^* \end{bmatrix}. \tag{4-8}$$

Then,

$$\begin{bmatrix} g_0 \\ g_1 \\ g_2 \\ g_3 \\ f_0 \\ f_1 \\ f_2 \\ f_3 \end{bmatrix} = [M]^{-1} \begin{bmatrix} \alpha_0^* \\ \alpha_1^* \\ \alpha_2^* \\ \alpha_3^* \\ \alpha_4^* \\ \alpha_5^* \\ \alpha_6^* \\ \alpha_7^* \end{bmatrix} \tag{4-9}$$

where,

$$[M] = \begin{bmatrix} 1 & 0 & 0 & 0 & 0 & 0 & 0 & 0 \\ \hat{\alpha}_1 & 1 & 0 & 0 & \hat{\beta}_1 & 0 & 0 & 0 \\ \hat{\alpha}_2 & \hat{\alpha}_1 & 1 & 0 & \hat{\beta}_2 & \hat{\beta}_1 & 0 & 0 \\ \hat{\alpha}_3 & \hat{\alpha}_2 & \hat{\alpha}_1 & 1 & \hat{\beta}_3 & \hat{\beta}_2 & \hat{\beta}_1 & 0 \\ \hat{\alpha}_4 & \hat{\alpha}_3 & \hat{\alpha}_2 & \hat{\alpha}_1 & \hat{\beta}_4 & \hat{\beta}_3 & \hat{\beta}_2 & \hat{\beta}_1 \\ 0 & \hat{\alpha}_4 & \hat{\alpha}_3 & \hat{\alpha}_2 & 0 & \hat{\beta}_4 & \hat{\beta}_3 & \hat{\beta}_2 \\ 0 & 0 & \hat{\alpha}_4 & \hat{\alpha}_3 & 0 & 0 & \hat{\beta}_4 & \hat{\beta}_3 \\ 0 & 0 & 0 & \hat{\alpha}_4 & 0 & 0 & 0 & \hat{\beta}_4 \end{bmatrix}$$

Adaptive control is achieved by continuously solving Equation (4-9) using values of $\hat{\alpha}_1$, $\hat{\alpha}_2$, $\hat{\alpha}_3$, $\hat{\alpha}_4$, $\hat{\beta}_1$, $\hat{\beta}_2$, $\hat{\beta}_3$, $\hat{\beta}_4$ determined by the parameter estimator. The resulting values of $g_0, g_2, g_2, g_3, f_0, f_1, f_2, f_3$, are used by the controller. Note that in real-time programing which calculation time cycle is seriously considered, $g_0, g_2, g_2, g_3, f_0, f_1, f_2, f_3$ can be expressed directly as functions of $\hat{\alpha}_1, \hat{\alpha}_2, \hat{\alpha}_3, \hat{\alpha}_4, \hat{\beta}_1, \hat{\beta}_2, \hat{\beta}_3, \hat{\beta}_4$ and the α^* values by solving Equation (4-8). This is to avoid matrix inversion of M in Equation (4-9).

4.3.2 Specification for $A_m(z)$

The characteristic Equation $A_m(z)$ is a 7th order system. Hence it is necessary to specify seven poles for $A_m(z)$. As discussed by Astrom & Wittenmark [1984] and others, only dominant poles need be specified. It must be recognized that by using the dominant pole approach, pole-zero cancellation occurs in the z-transfer function for the forced solution. The desired characteristic equation $A_m(z)$ is assumed to be second order, that is,

$$A_m(z) = 1 - 2\, e^{-\zeta \omega_n T} \cos \omega_n \sqrt{1-\zeta^2}\ z^{-1} + e^{-2\zeta \omega_n T}\, z^{-2}. \qquad (4\text{-}10)$$

Thus, $\alpha_0^* = 1$, $\alpha_1^* = -2\, e^{-\zeta \omega_n T} \cos \omega_n \sqrt{1-\zeta^2}$, and $\alpha_2^* = e^{-2\zeta \omega_n T}$. All other α^* values are set to zero. This forces the transfer function Y(z)/Yr(z) (Equation 4-2) to have 5 poles at z=0.

The characteristic equation $A_m(z)$ shown above corresponds to a second order continuous time system with a damping ratio ζ and a frequency ω sampled with period T.

The damping ratio ζ and frequency ω_n are determined from the desired rise-time and the maximum over-shoot of the system. The relationship are as shown below.

a. percentage overshoot to a step input is

$$\begin{cases} 100\left(1-\dfrac{\zeta}{0.5}\right), & 0<\zeta<0.4; \\ 100\left(\dfrac{1}{2}-\dfrac{\zeta}{1.6}\right), & 0.4<\zeta<0.8; \\ \equiv 0. & 0.8<\zeta. \end{cases} \tag{4-11}$$

b. rise time (time from 10% to 90% of the final value) is

$$\begin{cases} \dfrac{3\zeta}{\omega_n}, & 0.5<\zeta<0.9; \\ \dfrac{1}{\omega_n}[1+\zeta], & 0<\zeta<0.5. \end{cases} \tag{4-12}$$

To meet the desired step response requirements given in Section 2.2, the percentage overshoot and the rise time are taken as 5% and 10 second, respectively. The damping ratio ζ and frequency ω_n are 0.72 and 0.216. Simulation of the corresponding second order continuous system show that the percentage overshoot is 3.84 %, the rise time is 8.15 seconds.

For a sampling time of 0.25 seconds. The characteristic equation is $A_m(z) = 1 - 1.9224\, z^{-1} + 0.92518\, z^{-2}$.

4.3.3 Determination of T(z)

T(z) is designed to minimize the steady-state error in the tracking of the reference input signal (reference altitude). The z-transform of a step input reference signal is

$$Y_r(z) = c \cdot \frac{z}{z-1},$$

where, c is the step-input magnitude.

Applying the final value theorem, the steady state tracking error e_{ss} is give by

$$e_{ss} = \lim_{z \to 1} \frac{z-1}{z} \left[1 - \frac{B(z)\,T(z)}{A_m(z)} \right] Y_r(z)$$

$$= \lim_{z \to 1} \frac{z-1}{z} \left[1 - \frac{B(z)\,T(z)}{A_m(z)} \right] \cdot \frac{c \cdot z}{z-1}$$

$$= c \cdot \left(1 - \frac{B(1)T(1)}{A_m(1)} \right) \qquad (4\text{-}13)$$

For zero steady state input error,

$$T(1) = \frac{A_m(1)}{B(1)} = \frac{1 - 2\,e^{-\zeta \omega_n T} \cos \omega_n \sqrt{1-\zeta^2} + e^{-2\zeta \omega_n T}}{\hat{\beta}_1 + \hat{\beta}_2 + \hat{\beta}_3 + \hat{\beta}_4} \qquad (4\text{-}14)$$

Hence, T(z) is selected as a constant given by Equation (4-14).

4.4 Recursive Identification Algorithm

The inner loop design discussed in Section 4.2 is based on the assumption that the system parameters are known and constants. The pitch axis system parameters are identified on-line using the sampled input and output of the system.

Express Equation (4-1), the equation of the sampled data system, alternatively,

$$y(t) = \phi(t)^T \cdot \Theta(t); \tag{4-15}$$

where,

y(t) is the sampled-data output (altitude in feet);

u(t) is the calculated input signal the analog system (in feet);

$\phi(t)^T = (y(t-1), y(t-2), y(t-3), y(t-4), u(t-1), u(t-2), u(t-3), u(t-4))$;

$\Theta(t)^T = (-\hat{\alpha}_1, -\hat{\alpha}_2, -\hat{\alpha}_3, -\hat{\alpha}_4, \hat{\beta}_1, \hat{\beta}_2, \hat{\beta}_3, \hat{\beta}_4)$;

Note that $\phi(t)$ contains the sampled input and output data at the previous sampling intervals and $\Theta(t)$ is the identified system parameter vector at discrete time t.

As discussed in Section 2.1.3, the parameters of the linearized model are functions of the altitude, the speed and the weight of the aircraft. Therefore, the parameters of the sample data model are time-variant. Even during level flight, the parameters of the system are changing due to fuel comsumptions.

The identification of the time-varying parameters is accomplished using the recursive least-squares (RLS) algorithm with exponential discounting of old data. See Astrom [1983] and Astrom & Wittenmark [1984]. The RLS algorithm is shown in Equation (4-16) diagramed in Figure 4.2.

$$\begin{cases} \hat{y}(t) = \phi^T(t-1)\Theta(t-1); \\ \varepsilon(t) = y(t) - \hat{y}(t); \\ K(t) = P(t-1)\phi(t-1) / [1 + \phi(t-1)^T P(t-1)\phi(t-1)]; \\ \Theta(t) = \Theta(t-1) + K(t)\varepsilon(t); \\ P(t) = [I - K(t)\phi(t-1)^T]P(t-1) / \lambda; \end{cases} \tag{4-16}$$

where, $\hat{y}(t)$ is the predicted output at discrete time t;

$\varepsilon(t)$ is the predicted error at discrete time t;

K(t) is the estimation control gain;

λ is the forgetting factor;

P(t) is the covariance matrix;

$\phi(t)$ is the system vector which contains previous input and output data and $\Theta(t)$ is the identified system parameters, as expressed in Equation (4-2).

Note that the initial values for P(t) is taken as P(0)= I· d with d is a positive real value and I is a diagonal matrix of the same size of P(t). $\Theta(0)$ is taken as the system parameters at the time the adaptive control loop is activated. Details on the selection of d and $\Theta(0)$ for the pitch axis autopilot simulations are presented in Chapter V.

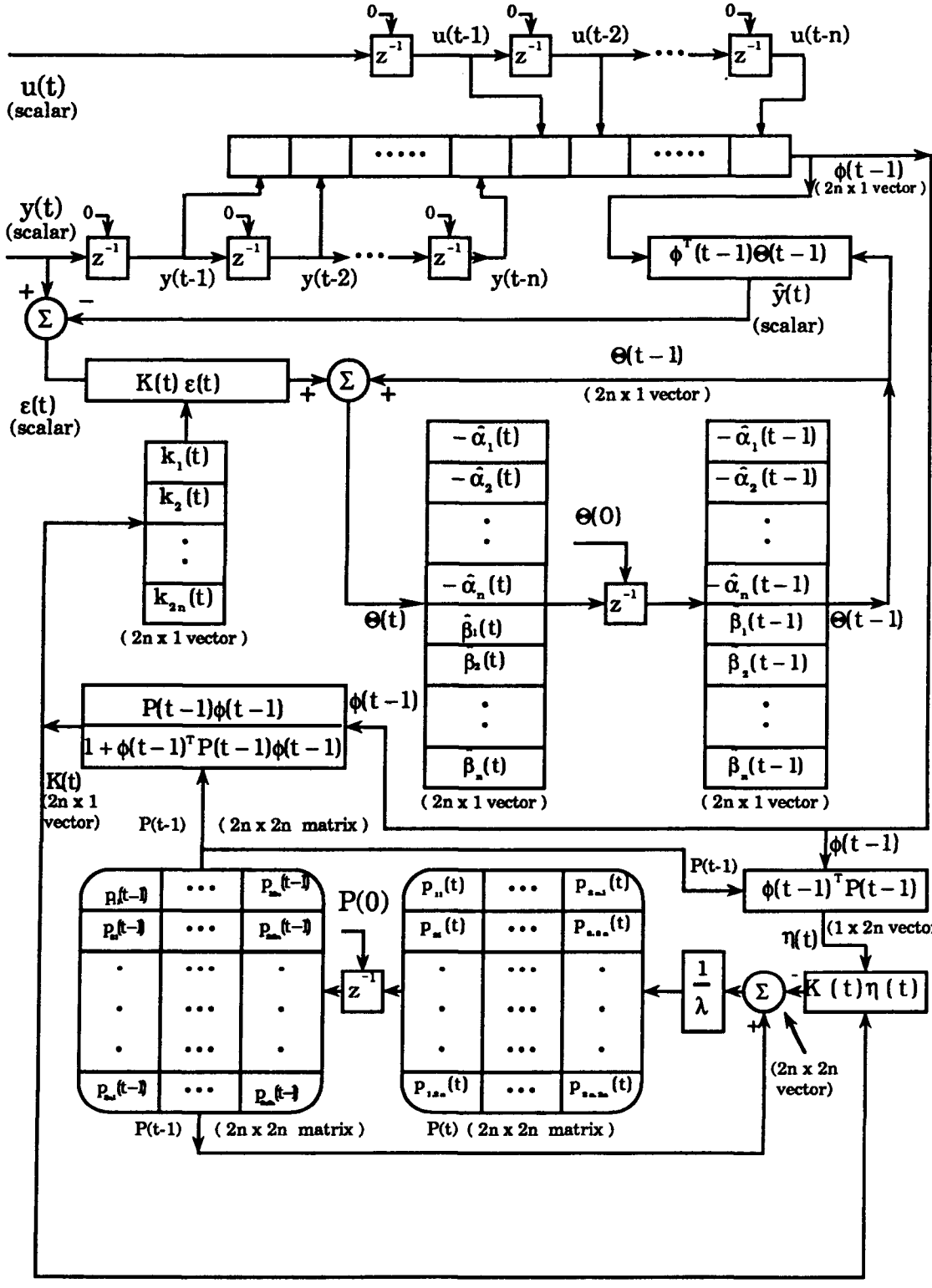

Figure 4.2 RLS System Parameter Identification Algorithm.

As shown in Figure 4.2, the system vector $\phi(t)$ is first updated with current input and output data. The estimated system output $\hat{y}(t)$ is calculated based on the system parameters estimated during last sampling period. The estimation error $\varepsilon(t)$, i.e., the difference between current output $y(t)$ and $\hat{y}(t)$, is then determined. The estimation control gain $K(t)$ is consequently calculated using the previous covariance matrix $P(t-1)$ and the system vector $\phi(t-1)$. The system parameters in $\Theta(t)$ are thus updated. The covariance matrix $P(t)$ is then calculated for the calculations during next sampling period. Details on the RLS are contained in Astrom [1983] and Astrom & Wittenmark [1984].

A weighting factor of less the unity ($\lambda<1$) is usually chosen. When $\lambda<1$, more recent data are weighted more than the old data. With λ much less than one, rapid discounting of old data results, which causes estimation uncertainty. If λ is taken to be very close to one, which implies that old data is not discounted rapidly, it is difficult to keep track of rapid parameter variations. The value of λ is related to how fast the system parameters are varying. The variation of the parameters of the aircraft is difficult to predict. So, the selection of λ for all conditions within a given flight envelope is indeed difficult.

Another disadvantage of using RLS is that identification of a time-varying system using a constant forgetting factor ($\lambda<1$) can generally result in estimator "blowing up", as discussed by Astrom & Wittenmark [1984] and Forescue *et al* [1981]. Since the recursive least-square algorithm (RLS) usually converges very fast, that is, $P(t)$ decreases

quickly, $P(t)\phi(t)$ in the RLS is thus approaching zero quickly. So, the estimation control gain K(t) approaches zero and the estimator switches off. Hence,

$$P(t) = [I-K(t)\phi(t-1)^T]\, P(t-1)/\lambda \approx P(t-1)/\lambda. \qquad (4\text{-}17)$$

Since $\lambda<1$, P(t) will become very large growing exponentially. The regulator is now very sensitive to any disturbance or to numerical error. A random input or set-point change will lead to a temporary unstable or complete unstable system, see Forescue *et al* [1981].

Due to the above reasons, the common RLS is not used for the design. Different identification algorithms has been introduced in Goodwin & Sin [1984] to remedy the problem with the exponential growth of P(t). In this thesis, the modified least-square algorithm proposed by Fortescue *et al* [1981] is used for the identification of the aircraft pitch axis system. As discussed in Fortescuse *et al* [1981], the modified least-square algorithm has two advantages: (1) the forgetting factor λ is calculated on-line such that the old data are discounted automatically; (2) P(t) is roughly prevented from being too small. Simulations have shown that the identification algorithm behaves well for time-varying chemical process, see Fortescue *et al* [1981].

The modified least-square algorithm is as shown in Equation (4-18) and diagramed in Figure 4.3. Note that Equation (4-18) is the same as Equation (4-16) except that the forgetting factor (λ) varies with time in Equation (4-18). Hence, the modified least-squares algorithm process system information is the same way as that of the RLS except that the forgetting factor λ is updated every sampling period prior to the

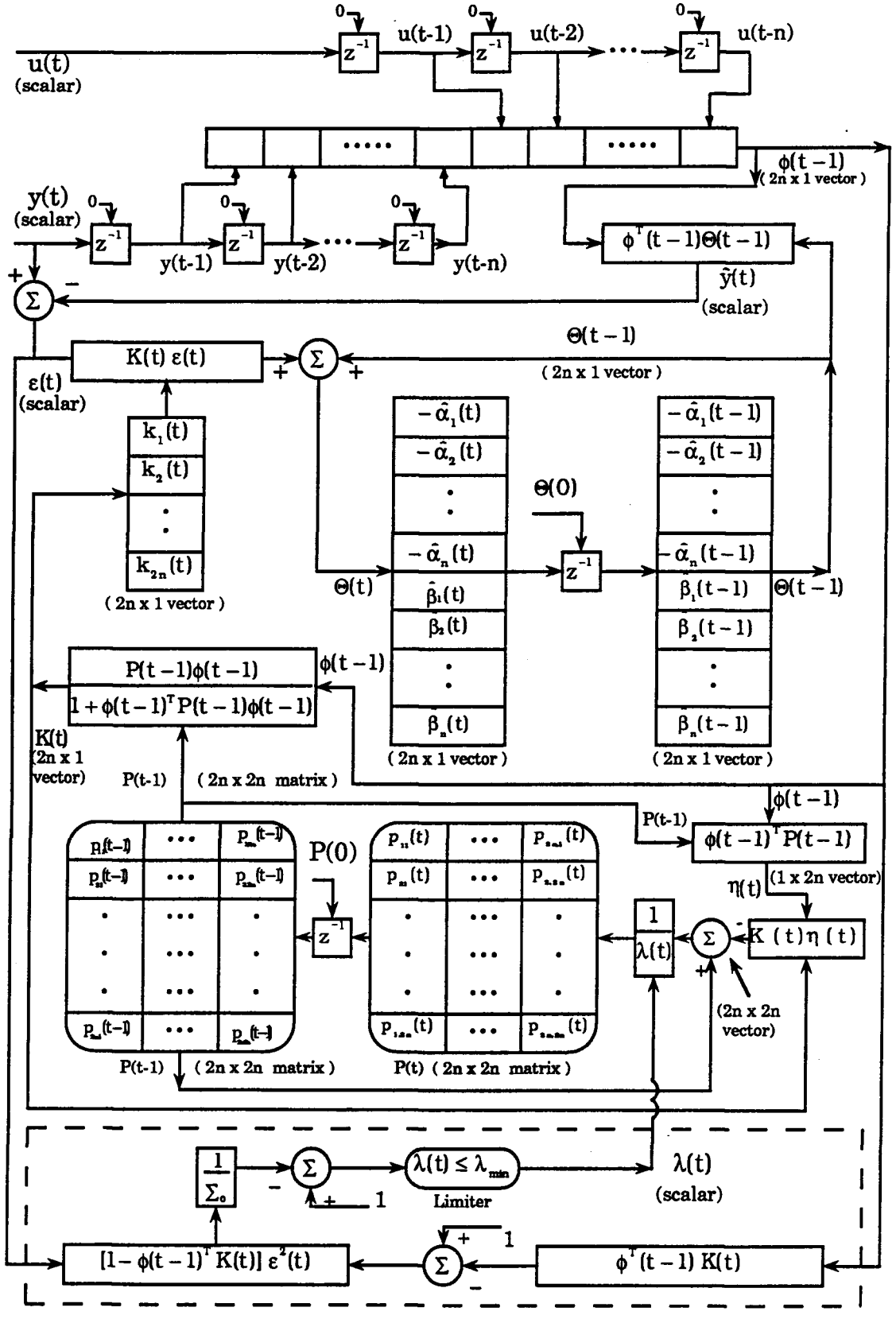

Figure 4.3 Modified RLS System Parameter Identification Algorithm.

calculation of the corvariance matrix P(t). The forgetting factor is bounded by λ_{min} to prevent λ from being too small. The time varying forgetting factor algorithm is framed with dash-lines in Figure 4.3.

$$\begin{cases} \hat{y}(t) = \phi^T(t-1)\Theta(t-1); \\ \varepsilon(t) = y(t) - \hat{y}(t); \\ K(t) = P(t-1)\phi(t-1) / [1 + \phi(t-1)^T P(t-1)\phi(t-1)]; \\ \Theta(t) = \Theta(t-1) + K(t)\varepsilon(t); \\ \lambda(t) = 1 - [1 - \phi(t-1)^T K(t)]\varepsilon^2(t) / \Sigma_0; \\ \lambda(t) \le \lambda_{min}, \lambda(t) = \lambda_{min}; \\ P(t) = [I - K(t)\phi(t-1)^T]P(t-1) / \lambda(t); \end{cases} \tag{4-18}$$

where, $\lambda(t)$ is the variable forgetting factor;

According to Fortescue *et al* [1981], the above algorithm is developed from the RLS under the consideration of information content of the estimator. For a near deterministic system the a posteriori error will at each step tell something about the system estimation. A small error implies that either the process has not been excited or there has been an excitation with a near correct set of parameter values or that the estimator is sensitive enough to significantly reduce the parameter error. For all these cases, it is reasonable to choose a forgetting factor close to unity to retain as much information as possible. On the other side, if the error is larger, the estimator sensitivity should be increased by choosing a lower forgetting factor. Based on these observations one can defined a measure of the information content as the weighted sum of the squares of the a posteriori errors. This can be expressed recursively as

$$\Sigma(t) = \lambda(t)\Sigma(t-1) + [1 - \phi(t-1)^T K(t)]\, \varepsilon^2(t) \tag{4-19}$$

which is the result of a rather lengthy derivation by Albert and Sittler [1966]. A strategy for choosing a forgetting factor may now be defined by keeping the information content $\Sigma(t)$ such that

$$\Sigma(t) = \Sigma(t-1) = \ldots\ldots\ldots\ldots = \Sigma_0$$

where Σ_0 is the expected information content. In other words, the amount of forgetting will at each step correspond to the amount of new information in the latest measure, thereby ensuring that the estimation is always based on the same amount information. Hence, from (4-19)

$$\begin{aligned}\lambda(t) &= \Sigma(t)/\Sigma(t-1) - [1-\phi(t-1)^T K(t)]\,\varepsilon^2(t)/\Sigma(t-1) \\ &= 1-[1-\phi(t-1)^T K(t)]\,\varepsilon^2(t)/\Sigma_0 \end{aligned} \qquad (4\text{-}20)$$

As discussed in Fortescue et al [1981], a smaller value of Σ_0 will give a large covariance matrix and a sensitive system; a larger value will give a less sensitive estimator and slow adaptation. In this design, the value for Σ_0 is determined from simulation studies.

CHAPTER 5

SIMULATION RESULTS

The schematic diagram of the adaptive pitch axis autopilot system is shown in Figure 5.1. It is basically the combination of the rate-feedback aircraft pitch axis system and the adaptive control loop.

5.1 The Simulation Configuration

Simulations are performed assuming the adaptive autopilot is activated after the aircraft has achieved level flight. The simulation of the system is a mixed system simulation which includes nonlinear integration of the rate-feedback pitch axis aircraft system and digital simulation of the adaptive control loop.

The Rung-Kutta-Mersion variable step size integration method is applied in the simulation of the pitch axis system shown in Equation (2-1). Since the adaptive autopilot turns on during level flight condition, the initial values for the system vector $[r, r', h, h', \theta, \theta']^T$ shown in Equation (2-1) are thus $[0, V_0, h_0, 0, \theta_0, 0]^T$, where V_0, h_0, and θ_0 are the speed, the altitude and the pitch angle at level flight, respectively. The thrust is set to that required for constant speed (V_0) level flight.

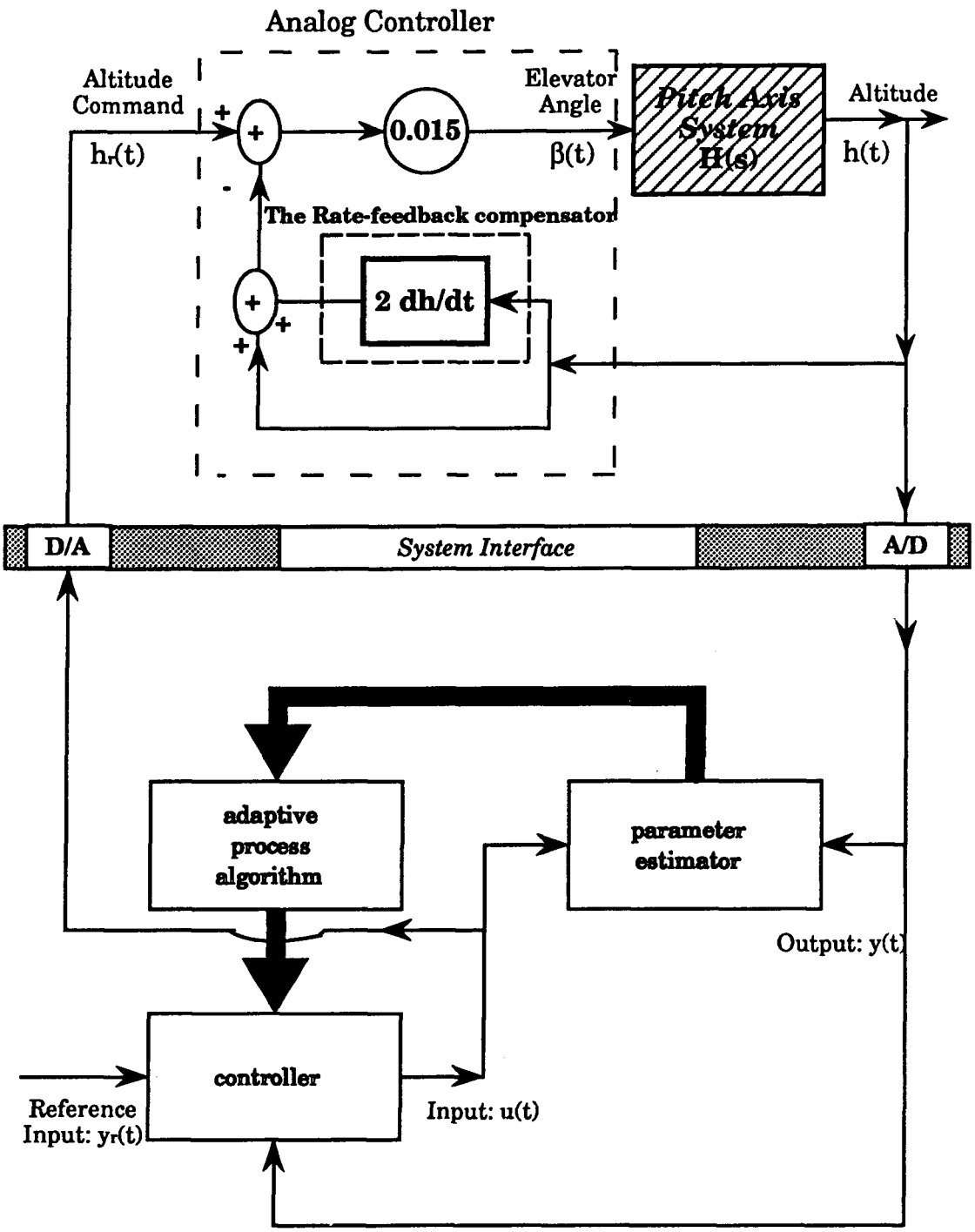

Figure 5.1 Schematic diagram for the pitch axis aircraft system with an adaptive autopilot.

In the identification of the system, the initial covariance matrix P(t) is taken as P(0)=100·I, where I is a diagonal matrix of the same size of P(t). The effect of P(0) is usually insignificant due to fast convergence of the least square algorithm. The best initial estimation of the system parameters is the level flight parameters. Thus, for the safety of the aircraft, the initial value for the parameter vector $\Theta(t)$ is $\Theta(0)=[\alpha_1^0, \alpha_2^0, \alpha_3^0, \alpha_4^0, \beta_1^0, \beta_2^0, \beta_3^0, \beta_4^0]$, where $\alpha_1^0, \alpha_2^0, \alpha_3^0, \alpha_4^0, \beta_1^0, \beta_2^0, \beta_3^0, \beta_4^0$ are the system parameters corresponding to level flight.

5.2 The Simulation Results

In the simulations, the aircraft using only the rate feedback controller is assumed flying horizontally at 0.7 Mach and 100 feet before the adaptive pitch axis autopilot is activated. The thrust at this flight condition is set 7,780 pounds. The weight of the aircraft is assumed to be 10,000 pounds. The elevator angle and pitangles are 0.507^0 and 1.014^0, respectively. At this flight condition, the 100 feet step command response of the rate-feedback pitch axis system is simulated as shown in Figures 5.2 (a) & (b). The maximum percentage overshoot, the rise time and the maximum acceleration of the system are 0.41%, 1.75 seconds and 50.83 feet/sec^2, respectively. The transient response of the system does not meet the desired requirements given in Section 2.2.

In the adaptive autopilot simulations, the reference altitude for tracking consists of two 100 feet step input commands and a ramp altitude command, as shown in Figure 5.3(a) & (b). The first command starts when the autopilot is activated. The second step command starts 86.5 seconds after the first command. The ramp altitude command starts at 174 seconds and goes up to 40,000 feet. The desired vertical speed for the ramp command is 100 feet/second, which corresponds to a flight path angle of about 7.35^0 degree. The first command is to test the system response when the adaptive control loop is activated. The second and the third commands test the system during adaptive autopilot operation. The sampling time is 0.25 seconds and the scalar quantity Σ_0=0.02 is used. The dominant characteristic equation is $A_m(z) = 1 - 1.9224\ z^{-1} + 0.92518\ z^{-2}$. As discussed in Section 4.3.2, the selection of $A_m(z)$ corresponds to a continuous second order system having the percentage overshoot of 3.84% and the rise time of 8.15 seconds.

(1) Step Command Responses

Figures 5.4 (a) through (c) show the altitude response, the tracking error and the vertical accelerations in adaptive tracking of the step commands. For the first step command, the maximum percentage overshoot is 4.21%, the rise time is 8.75 seconds, the maximum acceleration is 5.47 feet / sec^2. For the second step command, the maximum percentage overshoot is 3.80 %, the rise time is 8.75 seconds, and the maximum acceleration is 5.58 feet/sec^2. Thus, the transient response of the system satisfy the requirements. Note that the maximum percentage overshoot and the rise time are very close to those of a second order system having the dominant poles as specified for $A_m(z)$.

Figure 5.4(c) shows that the steady-state error is very small in tracking the horizontal flight altitude. For example, a 0.578% steady state error is obtained 86.5 seconds after the first command and 0.668% steady state error is obtained 120 seconds after the second command. Small level flight tracking error are thus achieved by the choice of T(z) in Section 4.3.3.

The forgetting factor (λ) in tracking the step commands is shown in Figure 5.5. It is observed that λ decreases to a lower value after the altitude command changes. λ changes slightly and increases (towards unity) during level flight. The variation of λ is due to the fact that altitude command change causes system parameter variations. When the system parameters change, the error between the system output and its estimation (based on previous system parameters), i.e., $\varepsilon(t)=y(t)-\hat{y}(t)$ as shown in Equation (4-17), becomes lager, Therefore, λ becomes smaller (this can be expected from Equation (4-17)). A smaller λ implies more old data is discount so that system parameter estimation can be updated. During level flight, the speed and altitude changes are very small. Furthermore, the weight loss (due to fuel consumption) is insignificant. The system parameters sustain small variations during level flight. So, a small drop in λ is observed after command changes. Note that λ approaches unity during level flight.

(2) Ramp Command Responses

Figure 5.6 (a) through (c) show the altitude response, the tracking error and the vertical acceleration for the ramp command.

As shown in Figure 5.6 (a), the altitude response follows the reference altitude command. Steady state tracking error is also observed due to the nature of the dominant closed-loop characteristic equation $A_m(z)$. The output of a time invariant stable second order linear system with a ramp_type input results in constant steady error. It is observed in Figure 5.6 (c) that the tracking error varies with time due to the adaptive controller not being to able to maintain the desired transfer function precisely during extreme altitude changes. Note that the system is the time-variant nonlinear pitch axis model shown in Equation 2.1.

As shown in Figure 5.6(b), the maximum vertical acceleration is less than 5.54 feet/sec^2, which satisfies the design requirement given in Section 2.2.

The forgetting factor λ for the ramp command tracking is shown in Figure 5.7. The forgetting factor drops to a lower value at the beginning of the command and then goes towards unity during tracking. However, λ drops after tracking for a certain time. Note the during the same time the tracking error between the actual flight altitude and the reference altitude gets smaller, which implies that the climbing rate is changing. The drop in λ keeps the tracking error from being too much different from the previous ones. Note that steady state output error results when a ramp signal is input to a second order system.

(3) The Elevator Angle and the Pitch Angle

Figure 5.8 (a) shows the elevator angle variations for the entire tracking while Figures 5.8 (b) gives a closer look to those corresponding to the step command changes and when the forgetting factor drops distinctly during the ramp command tracking. The elevator angle is found to be limited between 0.02^0 to 0.98^0. The pitch angle variation during the tracking is shown Figure 5.9. The range for the pitch angle variations is within 1.15^0 to 9.23^0. Note that the small elevator angle values satisfy the assumption of angles ($<15^0$) in deriving the system model in Appendix I.

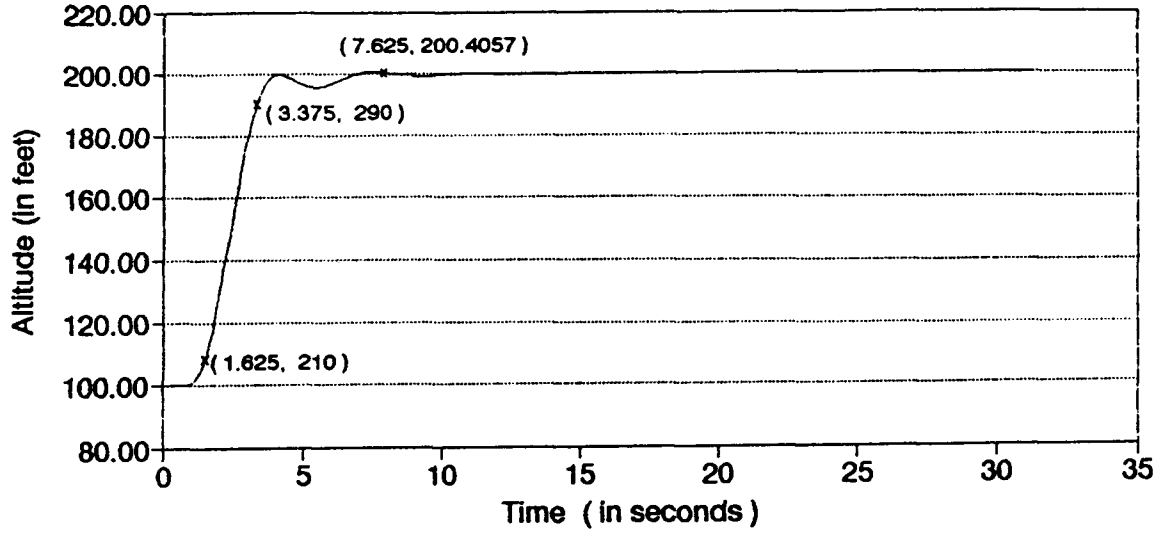

Figure 5.2(a) Step Response of the Rate-Feedback Pitch Axis System. W=10,000 pound; V=0.7 Mach; h=100 feet.

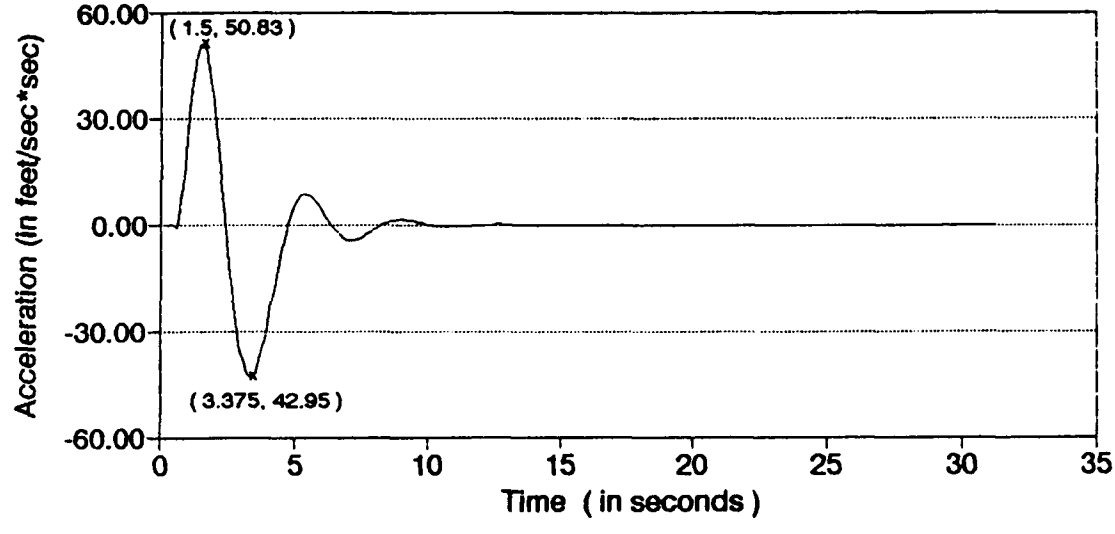

Figure 5.2(b) Vertical Acceleration of the Rate-Feedback Pitch Axis System. W=10,000 pound; V=0.7 Mach; h=100 feet.

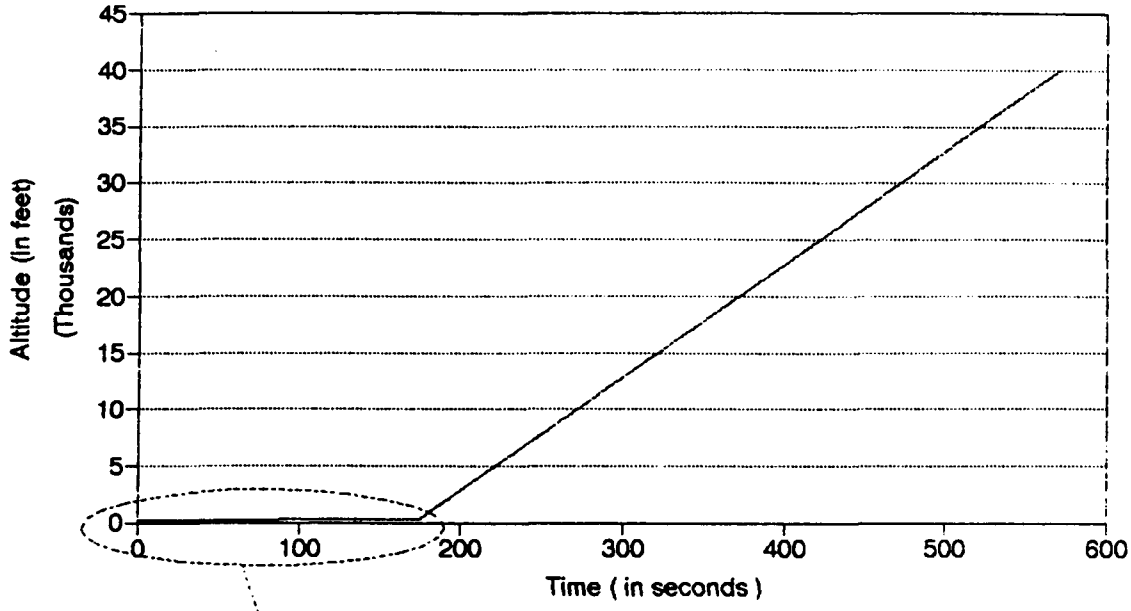

(1) Overall Reference Altitude;

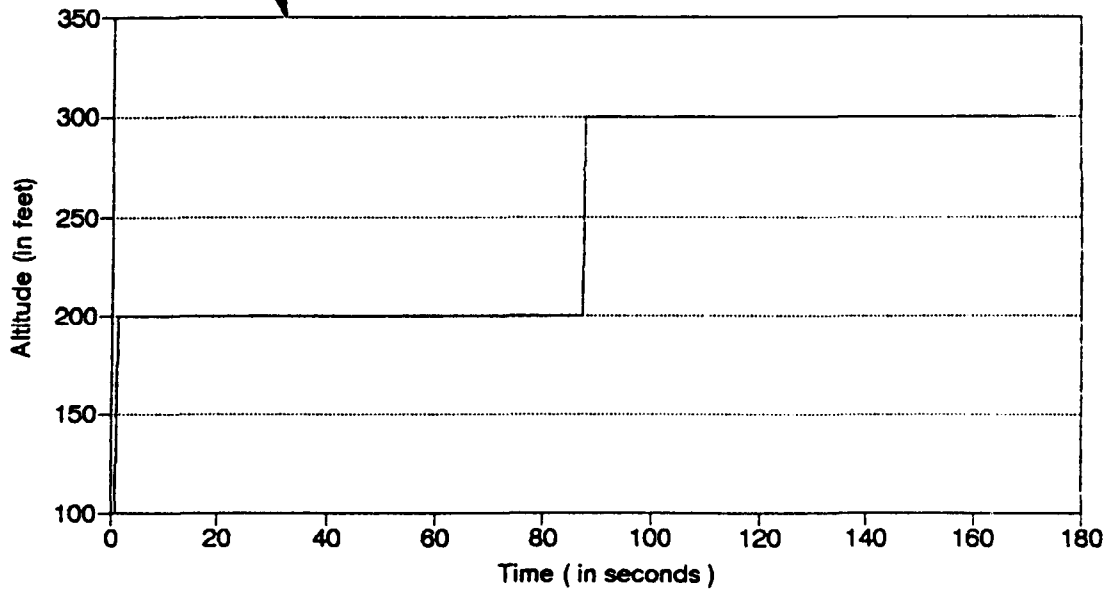

(2) The Step Commands;

Figure 5.3 The Reference Altitude Used for the Simulations.

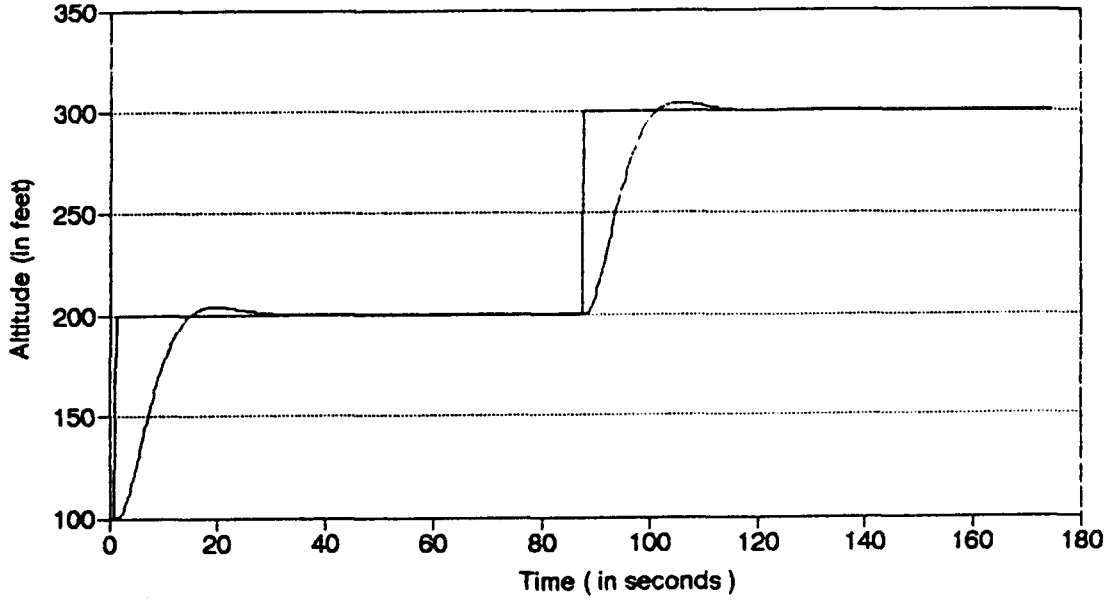

Figure 5.4(a) Adaptive Pitch Axis System Step Response.

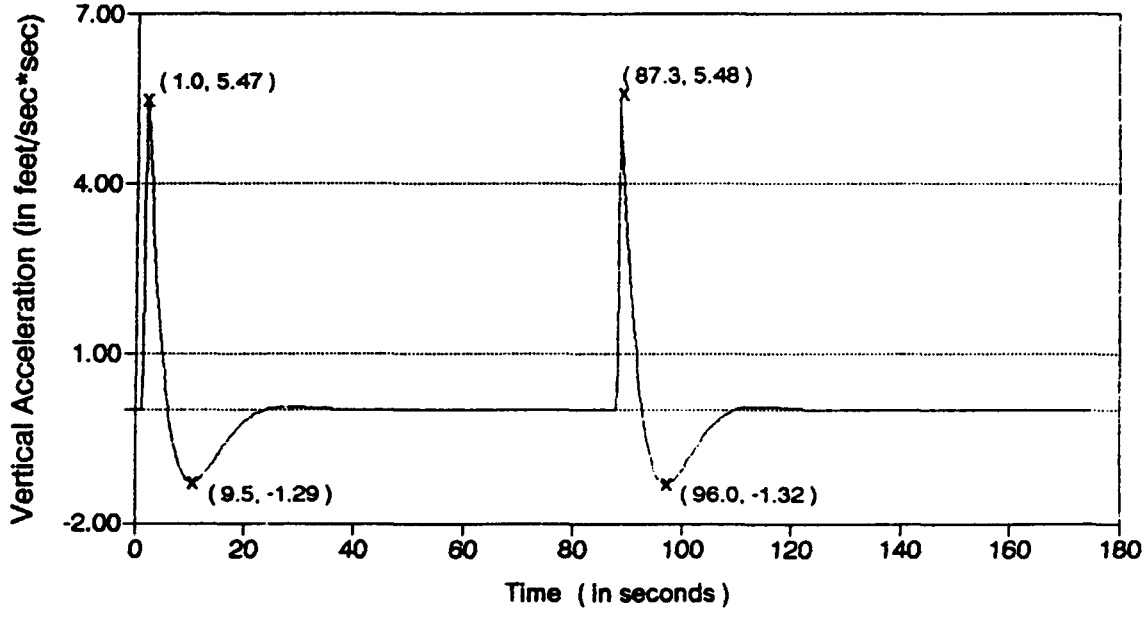

Figure 5.4(b) Vertical Acceleration in Adaptive Step Command Tracking.

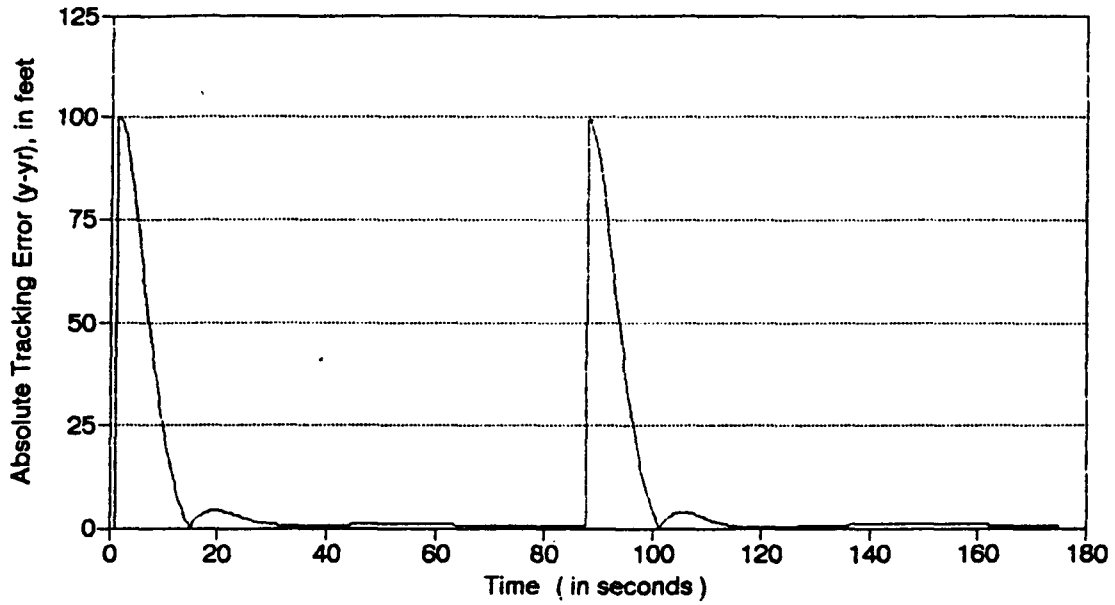

(1) Overall Absolute Tracking Error;

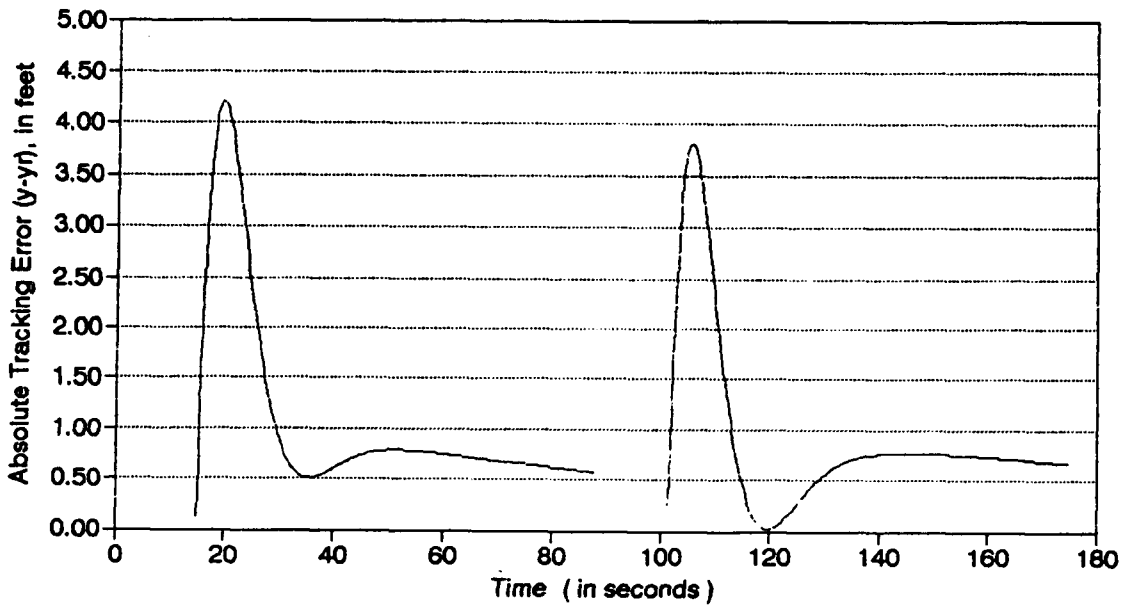

(2) The Absolute Tracking Error After the First Zero Error Value;

Figure 5.4(c) The Absolute Tracking Error in the Step Command Tracking.

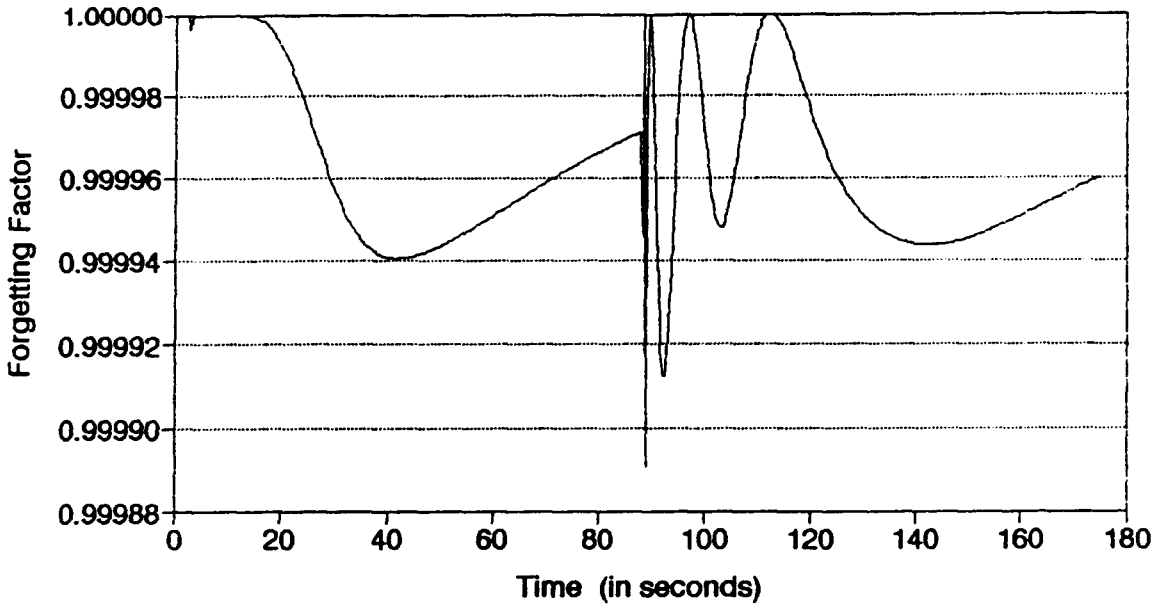

Figure 5.5 Forgetting Factor Variation in the Step Command Tracking.

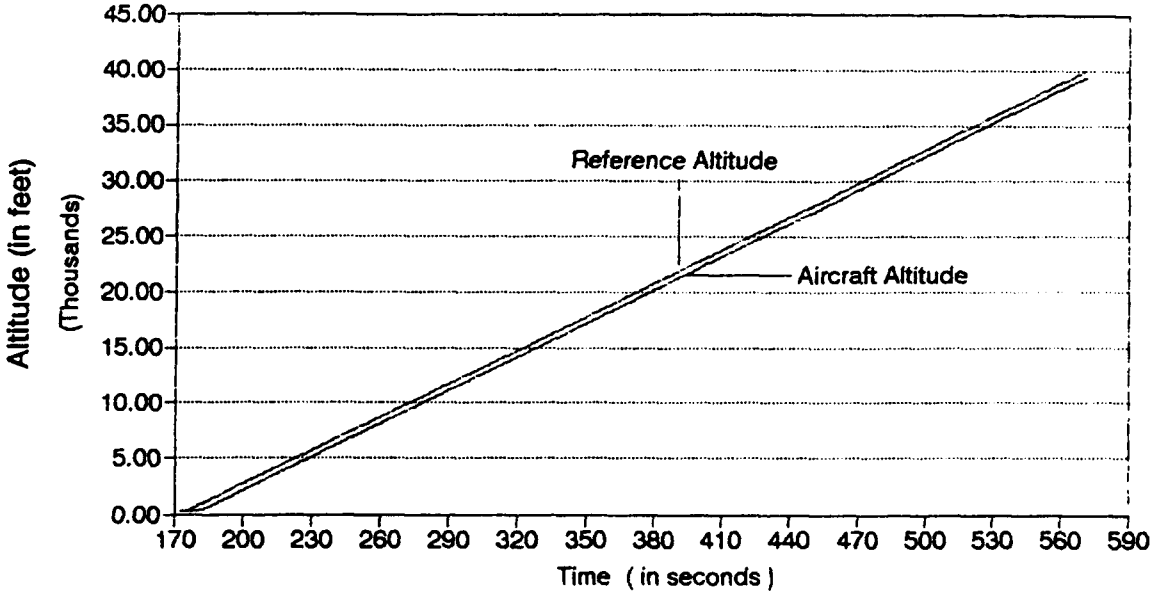

Figure 5.6(a) Altitude Response in Tracking the Ramp Command.

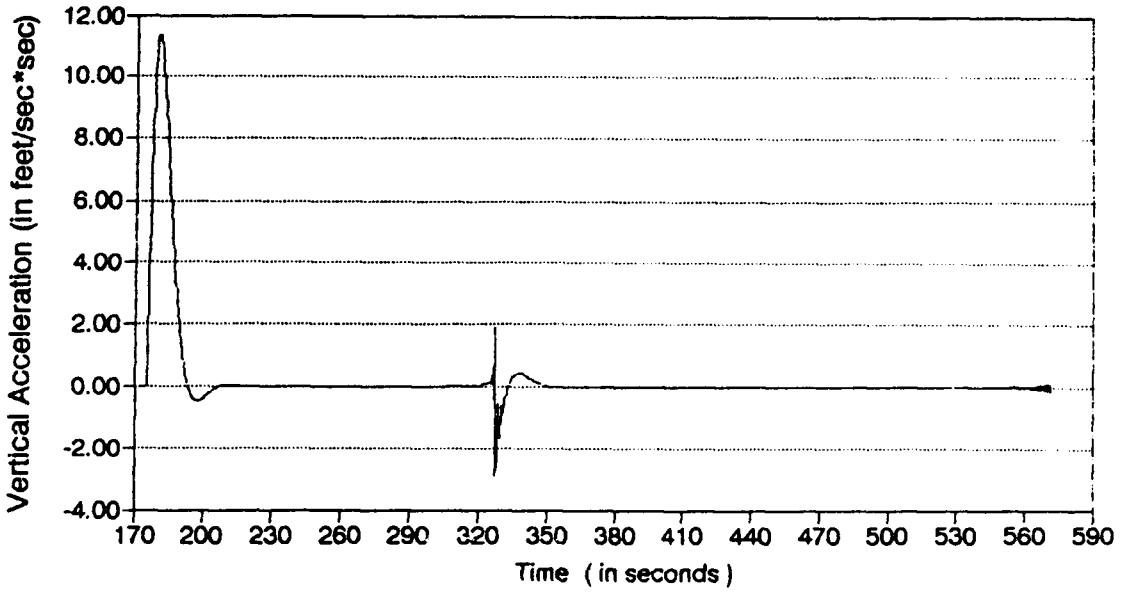

Figure 5.6(b) Vertical Acceleration in Adaptive Ramp Command Tracking.

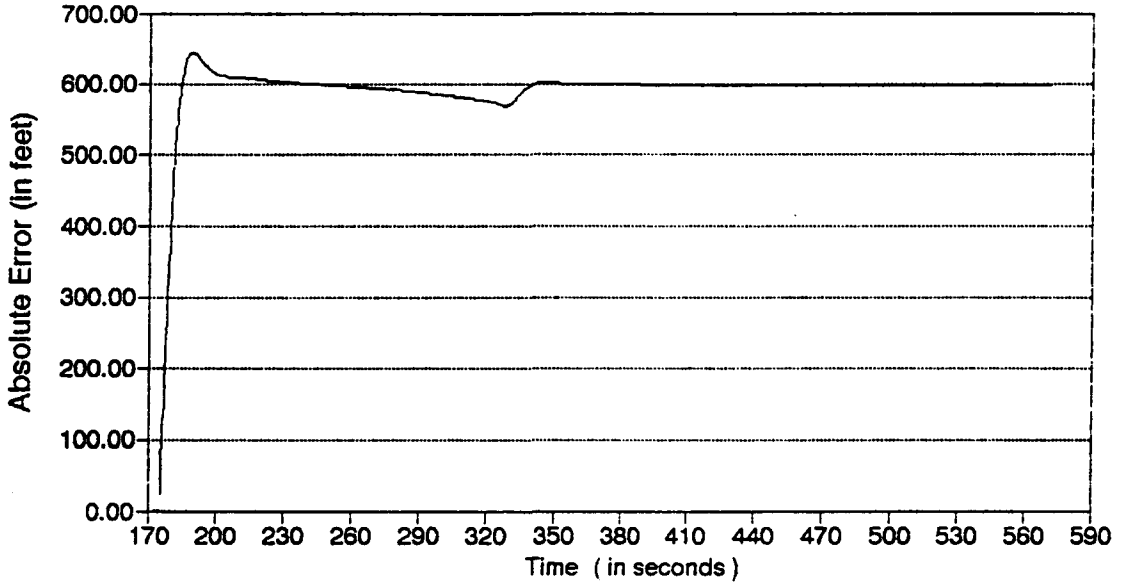

Figure 5.6(c) The Absolute Tracking Error in the Ramp Command Tracking.

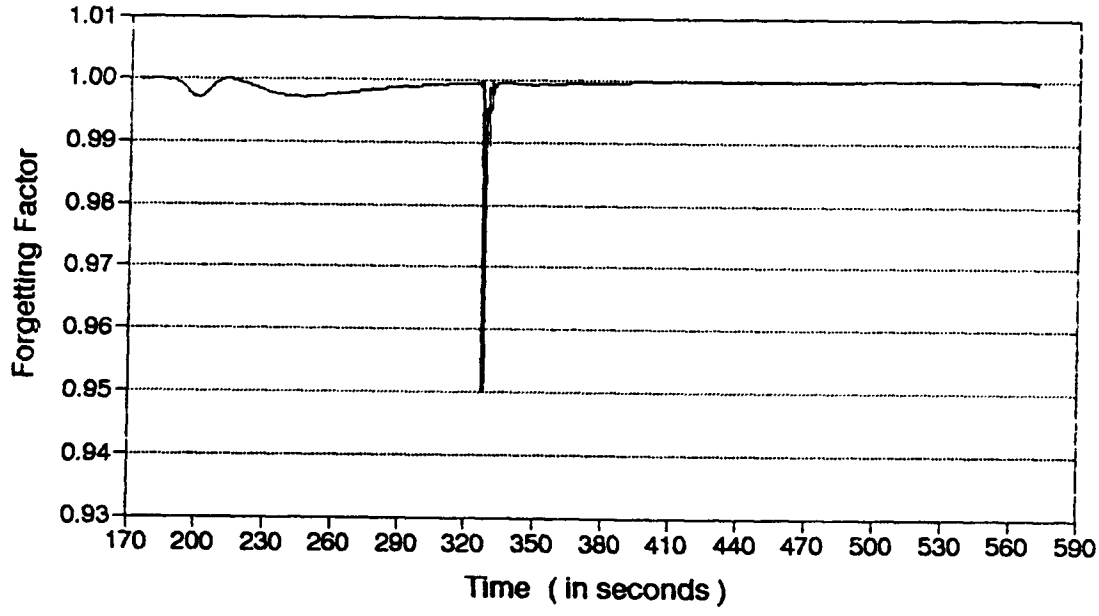

Figure 5.7 Forgetting Factor Variation in the Ramp Command Tracking.

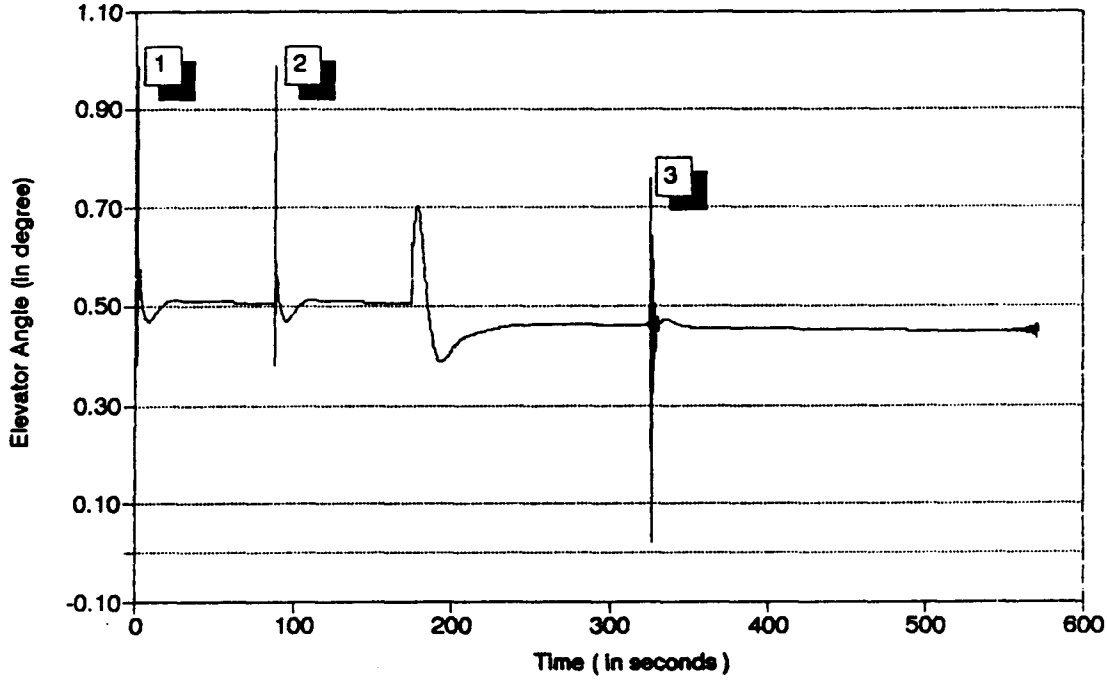

1 2 And 3 Indicating When the Elevator Has Relatively High Variations.

Figure 5.8(a) Elevator Angle Variation in the Entire Simulation.

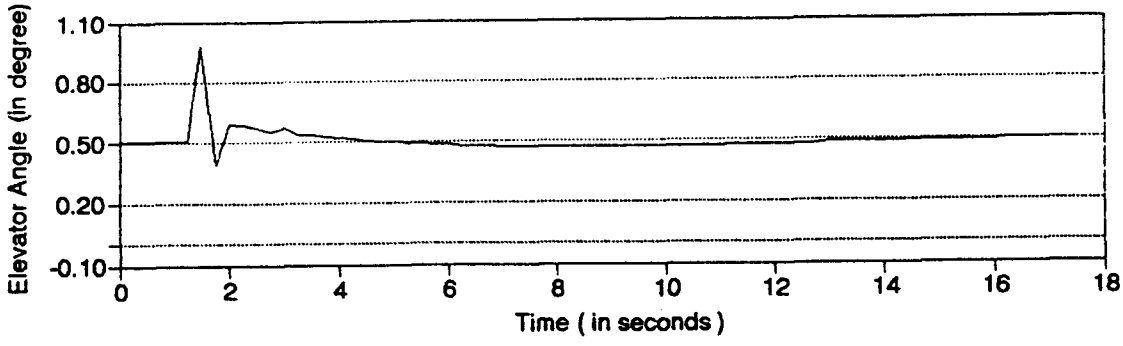

1 Elevator Angle For the First Step Command;

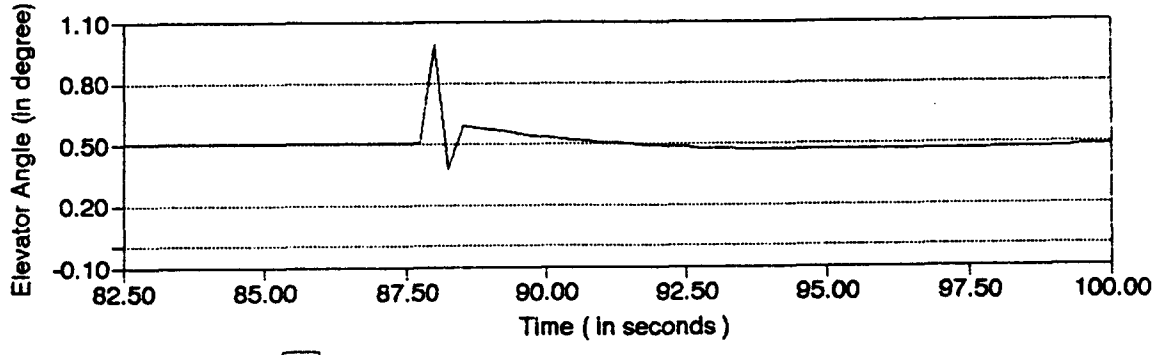

2 Elevator Angle For the Second Step Commnad;

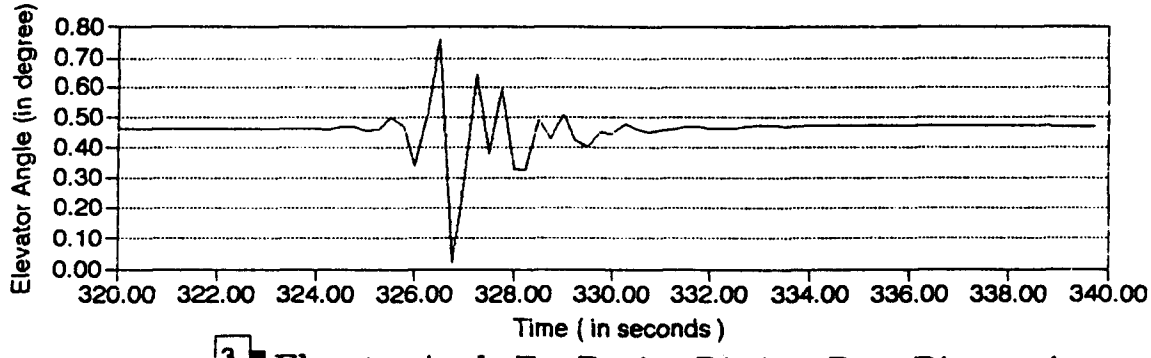

3 Elevator Angle For During Distinct Data Discounting;

Figure 5.8(b) Elevator Angle Variation for the Specific Time Segments.

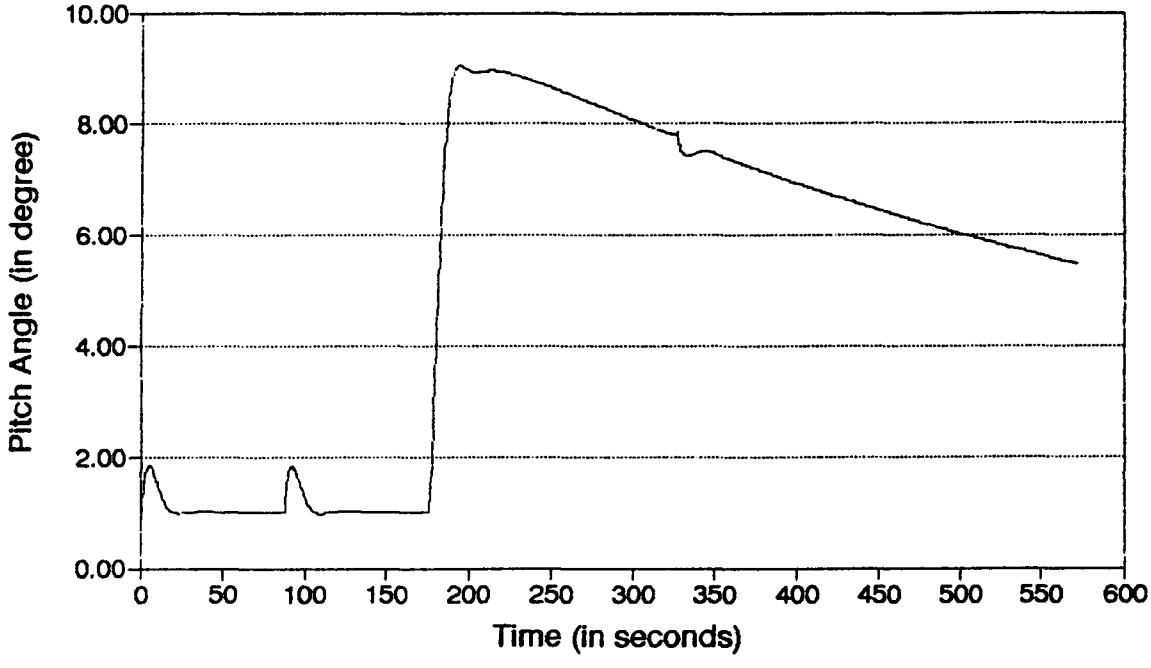

Figure 5.9 Pitch Angle Variation in the Entire Simulation.

CHAPTER 6

CONCLUSIONS

This thesis presents an adaptive autopilot design procedure for the aircraft pitch axis model in Appendix I. The design approach is based on the assumption that the adaptive autopilot is activated after the aircraft has achieved level flight. Chapter 3 shows that the level flight pitch axis system is unstable and has nonminimum phase. The flight pitch axis system is thus stabilized prior to the adaptive controller design using rate-feedback.

The rate-feedback configuration is applied to stabilize the pitch axis system within the desired flight envelope. The design method presented in Chapter 3 is based on assumption that if the system at the flight condition corresponding to the lowest dynamic pressure of the desired flight envelope is stabilized, then it is stabilized for the entire desired flight regime. Although the design criterion has been shown effective only for a particular flight envelope, it can serve as a starting point for different flight regimes. Note that the aerodynamic coefficients within the desired flight regime are assumed constants.

The adaptive controller design uses a pole-placement algorithm. The closed-loop system poles are placed to have the dominant poles corresponding to the poles of a second order system. The transient response of the system can then be determined approximately from the corresponding second order system. Desired system responses can be realized since the second order system characteristic polynomial, and

thus the poles, can be determined if the desired percentage overshoot and rise time are given. The discrete model for the pitch axis system is based on that of the level flight pitch axis system which has four poles. Simulation shows that the transient response is very close to that of the second order system having the dominant poles as specified. Further more, it is shown that the pole-placement algorithm can be applied to control nonminimum phase systems.

The pitch axis system is a time-varying system. A modified least square algorithm with a variable forgetting factor(λ) is used to estimate the system parameters. Simulations in Chapter 5 show that the variable forgetting factor (λ) is very active in updating system parameters whenever parameter variations occur. So, the modified least square algorithm with a variable forgetting factor(λ) is a proper choice in the estimation of the time-varying pitch axis model.

Simulation results indicate that the adaptive pitch axis autopilot is capable of tracking altitude commands after activation. Further work could involve studying the tracking performance when a disturbance occurs, minimizing the maximum elevator angle variation by selecting a proper sampling rate and the initial values for the parameter vector $\Theta(t)$, studying the effectiveness of the information content Σ_0 and the minimum forgetting factor λ_{min} of the modified least square algorithm to the tracking performance.

REFERENCES

Albert, A. and Sitter, R. W. (1966). "A Method for Computing Least Squares Estimates that Keep Up with the Data". SIAM J. Control, 3, 384.

Astrom, K. J. (1983). "Theory and Application of Adaptive Control ——— A survey". Automatica, Vol.19, No.5, pp513-528.

Astrom, K. J. and Wittenmark, B. (1980). "Self-tuning Controllers based on Pole-zero Placement". IEE Proceedings, Vol.127, Pt. D, No.3, May 1980, PP120-130.

Astrom, K. J. and Wittenmark, B. (1984). "Practical Issue in the Impletementation of Self-tuning Control". Automatica, Vol.20, No.5, PP595-605.

Astrom, K. J. and Wittenmark, B. (1990). Computer-Controlled Systems — Theory and Design. Prentice Hall, Englewood Cliffs, New Jersey.

Blakelock, J. H. [1965]. Automatic Control of Aircraft and Missiles. John Wiley & Sons, Inc., New York.

Clark, D. W. [1984]. "Self-tuning Control of Nonminimum-phase Systems". Automatica, vol.20, No.5, PP501-517.

Cordero, A. O. and Mayne, D. O. [1981]. "Deterministic convergence of a Self-tuning regulator with Variable Forgetting Factor". IEE Proc., Vol.128, Pt.D, No.1, PP19-23.

Elliot, J. R. [1977]. "NASA's Advanced Control Law Program for the F-8 Digital Fly-by-Wire Aircraft". IEEE Trans. Automat. Control, vol. Ac-22, No.5, PP753-757.

Fortescue, T. R., Kershenbaum, L.S. and Yastie, B. E. [1981]. "Impletementation of Self-tuning Regulators with Variable Forgetting Factors". Automatica, vol.16, No.6, PP831-835.

Goodwin, G. C. and Sin, K. S. [1981], "Adaptive Control of Nonminimum Phase Systems". IEEE Trans. Automat. Contr, AC-26, PP478-482.

Goodwin, G. C. and Sin, K. S. [1984], Adaptive Filtering Prediction and Control, Printice-Hall Inc., New Jersey.

Johnson, T. L. [1982]. "Self-Tuning Regulator Design for Adaptive Control of Aircraft Wing/Store Flutter". IEEE Trans. Automat. Contr. AC-27. No. 5. Oct.

Kuo, B. C. [1985]. Automatic Control Systems, 4th Edition. Prentice Hall of India. New Delhi.

Isermann, R. [1982]. "Parameter Adaptive control Algorithms ——— A tutorial". Automatica, Vol.18, No.5, PP501-517.

Norton, J. P. [1986]. An Introduction to Identification. Academic Press, London.

Saugen, J. L. [1987]. "Analog Longitudinal Aircraft Autopilot Design Using Root-locus Method". Project EE453. Oregon State University.

Appendices

APPENDIX I

The Aircraft Pitch Axis Model

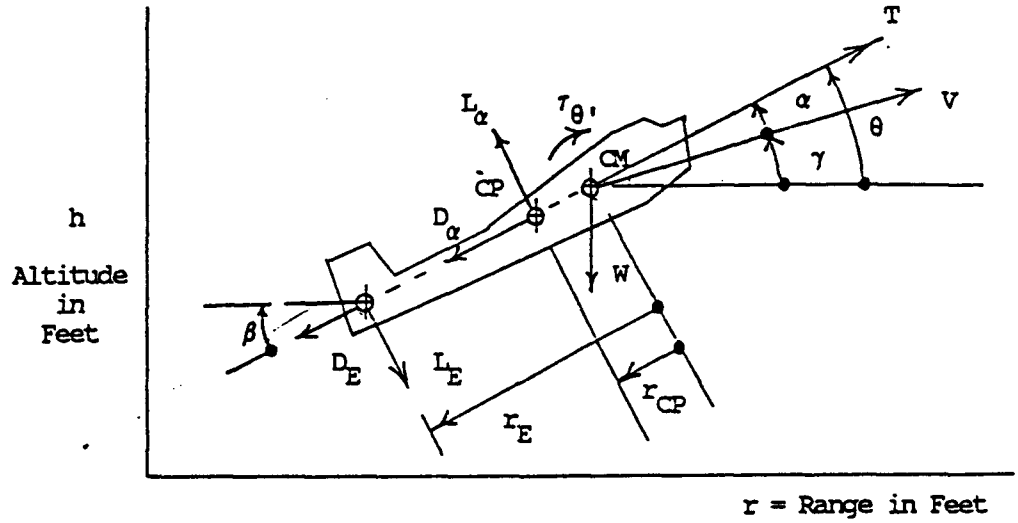

Figure AI.1 The Pitch Axis Aircraft Model.

h = Altitude in Feet, r = Range in Feet
θ = Pitch Angle in Radians
γ = Flight Path Angle in Radians
α = Angle of Attack in Radians
β = Elevator Deflection Angle in Radians
W = Weight in Pounds, T = Thrust in Pounds
J = Polar Moment of Inertia Around CM in Pound-Feet-Second^2/Radian
V = Velocity in Feet Per Second
CM = Center of Mass
CP = Center of Aerodynamic Pressure-No Elevator Deflection
r_{CP} = Distance from CM to CP in Feet
r_E = Distance from CM to Elevator Center of Aerodynamic Pressure in Feet

ρ = Atmospheric Density = $\rho_z \exp(-h/H)$ in Slugs/Cubic Foot
where ρ_z and H are the zero altitude density and exponential atmospheric factor, respectively.

A = Aerodynamic Shape Area in Square Feet
c = Aerodynamic Chord Length Factor in Feet
g = Acceleration Due to Earth = 32.2 Feet Per Second^2
m = Vehicle Mass = W/g in Slugs

L_α = Lift Force Due to α = $(0.5\ \rho\ V^2)\ A\ C_{l\alpha}\ \alpha$ in Pounds
D_α = Drag Force Due to α = $(0.5\ \rho\ V^2)\ A\ C_{d\alpha}$ in Pounds
L_E = Lift Force Due to β = $(0.5\ \rho\ V^2)\ A\ C_{l\beta}\ \alpha$ in Pounds
D_E = Drag Force Due to β = $(0.5\ \rho\ V^2)\ A\ C_{d\beta}$ in Pounds
$\tau_{\theta'}$ = Torque Around CM Due to θ' = $(0.5\ \rho\ V^2)\ Ac\ C_{m\theta'}\ \theta'$ in Pound-Feet

Assumptions:

-Vehicle dynamics can be adequately defined using a near earth inertial reference frame.
-The vehicle weight, thrust, lift and drag coefficients can all be assumed constants for the purpose of designing a pitch axis autopilot
-The locations of the CP, CM, and the elevator center of pressure are fixed.
-The parameters A and c are taken as unity for simplicity.
-Pitch, flight path, angle of attack, and elevator deflection angles can be assumed small (< 15 degrees) so that the following approximations can be made with small error (< 3.5%):

$$\cos\phi = 1,\ \sin\phi = \phi,\ \tan\phi = \phi$$

Equations of Motion:

$$r'' = \frac{T}{m}\cos\theta - \frac{(L_\alpha - L_E)}{m}\sin\theta - \frac{(D_\alpha + D_E)}{m}\cos\theta$$

$$h'' = \frac{T}{m}\sin\theta + \frac{(L_\alpha - L_E)}{m}\cos\theta - \frac{(D_\alpha + D_E)}{m}\sin\theta - g$$

$$\theta'' = -\frac{\tau_{\theta'}}{J} - \frac{L_\alpha r_{CP}}{J} + \frac{L_E r_E}{J}$$

where $\alpha = \theta - \sin^{-1}(h'/V)$

Equations of Motion Assuming Small Angles:

$$r'' = \frac{T}{m} - \frac{(L_\alpha - L_E)}{m}\theta - \frac{(D_\alpha + D_E)}{m}$$

$$h'' = \frac{T}{m}\theta + \frac{(L_\alpha - L_E)}{m} - \frac{(D_\alpha + D_E)}{m}\theta - g$$

$$\theta'' = -\frac{\tau_{\theta'}}{J} - \frac{L_\alpha r_{CP}}{J} + \frac{L_E r_E}{J}$$

where $\alpha = \theta - (h'/V)$

These equations can be put into the following form:

$$r'' = K_r - C_\alpha \alpha \theta - C_\beta \beta \theta$$

$$h'' = K_r \theta + C_\alpha \alpha - C_\beta \beta - g$$

$$\theta'' = - N_{\theta'} \theta' - N_\alpha \alpha + N_\beta \beta$$

where

$$K_r = \frac{T}{m} - \frac{1}{m}(0.5\rho V^2)\ (C_{d\alpha} + C_{d\beta})$$

$$C_\alpha = \frac{1}{m}(0.5\rho V^2)\ C_{l\alpha} \ ; \ C_\beta = \frac{1}{m}(0.5\rho V^2)\ C_{l\beta}$$

$$N_{\theta'} = \frac{1}{J}(0.5\rho V^2)\ C_{m\theta'} ; \ N_\alpha = \frac{m}{J}\ r_{CP}\ C_\alpha \ ; \ N_\beta = \frac{m}{J}\ r_E\ C_\beta$$

Note that these parameters are functions of T, V, m, and h assuming the aerodynamic coefficents are constants.

State Variable Model:

$$x^T = [\ r\ r'\ h\ h'\ \theta\ \theta'\ ] \ ; \ u = [\ \beta\ ] \ ; \ q^T = [\ h\ \theta\ ] \ ; \ \alpha = x_5 - \frac{x_4}{V}$$

$$x' = \begin{bmatrix} x_2 \\ K_r - C_\alpha \left(x_5 - \frac{x_4}{V} \right) x_5 + C_\beta u_1 x_5 \\ x_4 \\ K_r x_5 + C_\alpha \left(x_5 - \frac{x_4}{V} \right) - C_\beta u_1 - g \\ x_6 \\ -N_{\theta'} x_6 - N_\alpha \left(x_5 - \frac{x_4}{V} \right) + N_\beta u_1 \end{bmatrix} \qquad \text{(A.1)}$$

$$q = [\ x_3 \quad x_5\ ]$$

Operating Point Assumptions

The vehicle is flying horizontally at a constant velocity V at an altitude h_o. Thus the operating point flight path angle γ_o is zero and hence the operating point pitch angle θ_o and angle of attack α_o are equal but not zero. The range r is varying linearly with time, i.e. $r = Vt$ since the horizontal velocity is V and the vertical velocity is zero.

- The operating point elevator angle β_o is that which is required to maintain level flight.
- The vehicle thrust T and weight W are constants.
- The aerodynamic coefficients are constants.
- Dyhamical motion around the operating point for small angles is assumed not to change the magnitude of V significantly. However, r' and h' will change although r' is still assumed to be close to V.

Operating Point Conditions:

$$x_o^T = [\ Vt,\ V,\ h_o,\ 0,\ \theta_o,\ 0\ ]\ ;\ u_o = [\ \beta_o\ ]\ ;\ q^T = [\ h_o\ \theta_o\ ]$$

$$x' = \begin{bmatrix} r_o' \\ 0 \\ 0 \\ 0 \\ 0 \\ 0 \end{bmatrix} = \begin{bmatrix} V \\ K_r - C_\alpha \theta_o^2 + C_\beta \beta_o \theta_o \\ 0 \\ K_r \theta_o + C_\alpha \theta_o - C_\beta \beta_o - g \\ 0 \\ -N_\alpha \theta_o + N_\beta \beta_o \end{bmatrix} \qquad \text{(A.2)}$$

The three non-trivial equations above are solved for θ_o, β_o, and the thrust T with the following results:

$$\rho_o = \rho_z \exp(-h_o/H)$$

$$\theta_o^3 + \theta_o = \frac{W}{(0.5\rho_o V^2)\ C_{l\alpha}} \left[\frac{r_E}{r_E - r_{CP}} \right]$$

$$\beta_o = \frac{r_{CP}\ C_{l\alpha}}{r_E\ C_{l\beta}}\ \theta_o \qquad \text{(A.3)}$$

$$K_{ro} = (0.5\rho_o V^2)\ C_{l\alpha}\ \left(1 - \frac{r_{CP}}{r_E} \right)$$

$$T = m K_{ro} + (0.5\rho_o V^2)\ (C_{d\alpha} + C_{d\beta})$$

Linearized State Variable Model Around the Operating Point:

$$\delta x' = \begin{bmatrix} 0 & 1 & 0 & 0 & 0 & 0 \\ 0 & 0 & a_{23} & a_{24} & a_{25} & 0 \\ 0 & 0 & 0 & 1 & 0 & 0 \\ 0 & 0 & a_{43} & a_{44} & a_{45} & 0 \\ 0 & 0 & 0 & 0 & 0 & 1 \\ 0 & 0 & a_{63} & a_{64} & a_{65} & a_{66} \end{bmatrix} \delta x + \begin{bmatrix} 0 \\ b_2 \\ 0 \\ b_4 \\ 0 \\ b_6 \end{bmatrix} \delta u \qquad \text{(A.4)}$$

$$\delta q = [\, 1 \quad 1 \,]\, \delta x$$

where $x = x_o + \delta x$, $u = u_o + \delta u$

The a and b parameters are given by the following:

$$\begin{cases} DP = \rho_z \exp(-ho/H);\ DPM = DP/m;\ DRJ = DP/J;\ DPMV = DPM/V;\ DRJV = DRJ/V \\ DPDH = -DP/H;\ DPDHM = DPDH/m;\ DPDHJ = DPDH/J \\ b_2 = DPM\, C_{l\beta}\, \theta_o\ ;\ b_4 = -DPM\, C_{l\beta}\ ;\ b_6 = DRJ\, rE\, C_{l\beta} \\ a_{23} = DPDHM\, [\, -(C_{d\alpha} + C_{d\beta}) + C_{l\alpha}\theta_o^{\,2} + C_{l\beta}\beta_o\theta_o \,] \\ a_{24} = DPMV\, C_{l\alpha}\, \theta_o \\ a_{25} = DPM\, [\, -2\, C_{l\alpha}\theta_o + C_{l\beta}\beta_o \,] \\ a_{43} = DPDHM\, [\, (C_{l\alpha} - C_{d\alpha} - C_{d\beta})\theta_o - C_{l\beta}\beta_o \,] \\ a_{44} = -DPMV\, C_{l\alpha} \\ a_{45} = T/m + DPM\, [\, C_{l\alpha} - C_{d\alpha} - C_{d\beta} \,] \\ a_{63} = DPDHJ\, [\, -r_{CP}C_{l\alpha}\theta_o + r_E C_{l\beta}\beta_o \,] \\ a_{64} = DRJV\, r_{CP}\, C_{l\alpha} \\ a_{65} = -DRJ\ \ r_{CP}\, C_{l\alpha} \\ a_{66} = -DRJ\ \ C_{m\theta'} \end{cases} \qquad \text{(A.5)}$$

APPENDIX II

Derivation of the Pitch Axis System Transfer Function

This appendix shows the details of obtaining Equation (2-4) from Equation (2-3). The derivation uses the signal-flow graph of Equation (2-3). Further information on signal-flow graph method is referred to Kuo [1985].

The procedure for obtain Equation (2-4) is:

1. draw the signal flow graph of Equation (2-3);
2. find the transfer function H(s) using the general gain formula,

$$M = \frac{y_{out}}{y_{in}} = \sum_{k=1}^{N} \frac{M_k \Delta_k}{\Delta}$$

where, M=gain between the input and output nodes, i.e., H(s);

N=total number of forward paths;

M_k=gain of the kth forward path;

$\Delta = 1 - P_{m1} + P_{m2} - P_{m3} + ...$

P_{mr}=gain product of the *m*th possible combination of r nontouching loops.

Further details are referred to Kuo [1985].

The signal flow graph of Equation (2-3) is shown in Figure II.1. There are two paths from the input node u(s) to the output node X_3 (s). By following the above procedure, Equation (2-3) is found as shown below.

$$M_1\Delta_1 = \frac{1}{s}\frac{a_{45}}{s-a_{44}}\frac{1}{s}\frac{b_6}{s-a_{66}};$$

$$M_2\Delta_2 = \frac{1}{s}\frac{b_4}{s-a_{44}}\left(1-\frac{a_{65}}{s(s-a_{66})}\right);$$

$$\Delta = 1+\frac{1}{s}\frac{a_{66}}{s-a_{66}}\frac{1}{s}\frac{a_{43}}{s-a_{44}}-\frac{a_{65}}{s(s-a_{66})}-\frac{a_{43}}{s(s-a_{44})}-\frac{1}{s}\frac{a_{45}}{s-a_{44}}\frac{a_{64}}{s-a_{66}}-\frac{1}{s}\frac{a_{45}}{s-a_{44}}\frac{1}{s}\frac{a_{64}}{s-a_{66}};$$

So, the transfer function H(s) is,

$$H(s) = \frac{\delta h(s)}{\delta\beta(s)} = \frac{\delta x_3(s)}{\delta u(s)} = \sum_{k=1}^{N}\frac{M_k\Delta_k}{\Delta}$$

$$= \frac{\left(\frac{1}{s}\frac{a_{45}}{s-a_{44}}\frac{1}{s}\frac{b_6}{s-a_{66}}\right) + \left(\frac{1}{s}\frac{b_4}{s-a_{44}}\left(1-\frac{a_{65}}{s(s-a_{66})}\right)\right)}{1+\frac{1}{s}\frac{a_{66}}{s-a_{66}}\frac{1}{s}\frac{a_{43}}{s-a_{44}}-\frac{a_{65}}{s(s-a_{66})}-\frac{a_{43}}{s(s-a_{44})}-\frac{1}{s}\frac{a_{45}}{s-a_{44}}\frac{a_{64}}{s-a_{66}}-\frac{1}{s}\frac{a_{45}}{s-a_{44}}\frac{1}{s}\frac{a_{64}}{s-a_{66}}}$$

$$= \frac{a_{45}b_6+b_4(s^2-a_{66}s-a_{65})}{(s-a_{44})(s-a_{66})s^2+a_{65}a_{43}-a_{65}s(s-a_{44})-a_{43}s(s-a_{66})-a_{45}a_{64}s-a_{45}a_{63}}$$

$$= \frac{b_4s^2-b_4a_{66}s+a_{45}b_6-a_{65}b_4}{s^4-(a_{44}+a_{66})s^3+(a_{44}a_{66}-a_{65}-a_{43})s^2+(a_{65}a_{44}+a_{66}a_{43}-a_{45}a_{64})s+a_{65}a_{43}-a_{63}a_{45}}$$

(2-4)

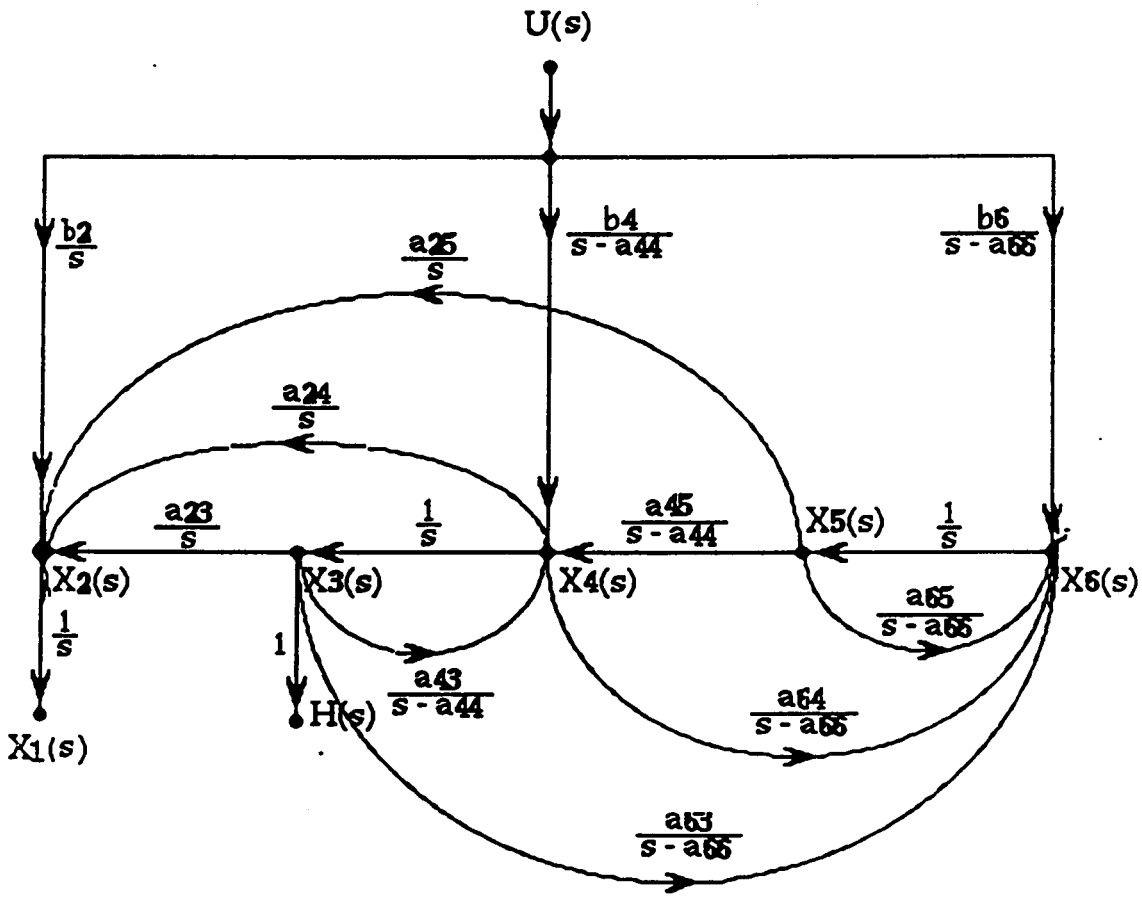

Figure AII.1 The Signal Flow Graph of Equation (2-3).

APPENDIX III

Theorem 5.3.1 of Goodwin & Sin [1984]

This appendix gives the description of Theorem 5.3.1 of Goodwin & Sin [1984].

Theorem 5.3.1: If $A(q^{-1})$ and $B(q^{-1})$ are relatively prime and n=maximum degree($A(q^{-1})$, $B(q^{-1})$), any arbitrary polynomial $A^*(q^{-1})$ of degree (2n-1) can be obtained as the sum $A(q^{-1})L(q^{-1})+B(q^{-1})P(q^{-1}) = A^*(q^{-1})$ for unique polynomials $L(q^{-1})$ and $P(q^{-1})$ of degree(n-1).

The above theorem implies: provide that $A(q^{-1})$ and $B(q^{-1})$ are relatively prime and n=maximum degree($A(q^{-1})$, $B(q^{-1})$), $L(q^{-1})$ and $P(q^{-1})$ can be found by assuming that they have degrees of (n-1), i.e.,

$$L(q^{-1}) = l_0 + l_1 \cdot q^{-1} + l_2 \cdot q^{-2} + \ldots\ldots\ldots + l_{n-1} \cdot q^{-(n-1)};$$
$$P(q^{-1}) = p_0 + p_1 \cdot q^{-1} + p_2 \cdot q^{-2} + \ldots\ldots\ldots + p_{n-1} \cdot q^{-(n-1)}$$

The procedure of solving the Duphantine Equation $A(q^{-1})L(q^{-1}) + B(q^{-1})P(q^{-1}) = A^*(q^{-1})$ would then be:

if,

$$A^*(q^{-1}) = A_m(q^{-1})A_0(q^{-1}) = \alpha_0^* + \alpha_1^* \cdot q^{-1} + \alpha_2^* \cdot q^{-2} + \ldots\ldots\ldots + \alpha_{2n-1}^* \cdot q^{-(2n-1)};$$

equating coefficients on either side of the Duphantine Equation gives:

$$\begin{bmatrix} \alpha_0 & 0 & 0 & 0 & 0 & \beta_0 & 0 & 0 & 0 & 0 \\ \alpha_1 & \alpha_0 & 0 & 0 & 0 & \beta_1 & \beta_0 & 0 & 0 & 0 \\ . & \alpha_1 & . & 0 & 0 & . & \beta_1 & . & 0 & 0 \\ . & . & . & . & 0 & . & . & . & . & 0 \\ . & . & . & . & \alpha_0 & . & . & . & . & \beta_0 \\ \alpha_n & . & . & . & \alpha_1 & \beta_n & . & . & . & \beta_1 \\ 0 & \alpha_n & . & . & . & 0 & \beta_n & . & . & . \\ 0 & 0 & . & . & . & 0 & 0 & . & . & . \\ 0 & 0 & 0 & . & . & 0 & 0 & 0 & . & . \\ 0 & 0 & 0 & 0 & \alpha_n & 0 & 0 & 0 & 0 & \beta_n \end{bmatrix} \begin{bmatrix} l_0 \\ l_1 \\ . \\ . \\ l_{n-1} \\ p_0 \\ p_1 \\ . \\ . \\ p_{n-1} \end{bmatrix} = \begin{bmatrix} \alpha_0^{\bullet} \\ \alpha_1^{\bullet} \\ \alpha_2^{\bullet} \\ . \\ . \\ . \\ . \\ . \\ . \\ \alpha_{2n-2}^{\bullet} \\ \alpha_{2n-1}^{\bullet} \end{bmatrix};$$

$$\text{Then,} \begin{bmatrix} l_0 \\ l_1 \\ . \\ . \\ l_{n-1} \\ p_0 \\ p_1 \\ . \\ . \\ p_{n-1} \end{bmatrix} = Me^{-1} \begin{bmatrix} \alpha_0^{\bullet} \\ \alpha_1^{\bullet} \\ \alpha_2^{\bullet} \\ . \\ . \\ . \\ . \\ . \\ . \\ \alpha_{2n-2}^{\bullet} \\ \alpha_{2n-1}^{\bullet} \end{bmatrix};$$

$$\text{Where, Me} = \begin{bmatrix} \alpha_0 & 0 & 0 & 0 & 0 & \beta_0 & 0 & 0 & 0 & 0 \\ \alpha_1 & \alpha_0 & 0 & 0 & 0 & \beta_1 & \beta_0 & 0 & 0 & 0 \\ . & \alpha_1 & . & 0 & 0 & . & \beta_1 & . & 0 & 0 \\ . & . & . & . & 0 & . & . & . & . & 0 \\ . & . & . & . & \alpha_0 & . & . & . & . & \beta_0 \\ \alpha_n & . & . & . & \alpha_1 & \beta_n & . & . & . & \beta_1 \\ 0 & \alpha_n & . & . & . & 0 & \beta_n & . & . & . \\ 0 & 0 & . & . & . & 0 & 0 & . & . & . \\ 0 & 0 & 0 & . & . & 0 & 0 & 0 & . & . \\ 0 & 0 & 0 & 0 & \alpha_n & 0 & 0 & 0 & 0 & \beta_n \end{bmatrix};$$

Further details on the proof of the theorem is referred to Goodwin & Sin [1984].